Investigation into Ship Roll Hydrodynamic Coefficients using Motion Simulations

by

Seyedsadreddin (Sadra) Kianejadtejenaki

National Centre for Ports and Shipping

Australian Maritime College

Submitted in fulfilment of the requirements for the degree of Doctor of Philosophy

University of Tasmania

July 2019

Declarations

Declaration of Originality

This thesis contains no material that has been accepted for a degree or diploma by the university or other institution. To the best of my knowledge and belief, this thesis contains no material previously published or written by another person, except where due acknowledgement is made in the text.

Authority of Access

This thesis may be available for the loan and limited copying and communication in accordance with the Copyright Act 1968.

Signed:

Seyedsadreddin Kianejadtejenaki

Date: 08/07/2019

Statement of Published Work Contained in Thesis

The publishers of the papers comprising Chapters 2 to 5 hold the copyright, and for that content, and access to the material should be sought from the respective journals. The remaining non-published content of the thesis, and chapters 6 and 7 are submitted and are under review, and may be made available for loan and limited copying and communication in accordance with the Copyright Act 1968.

Statement of Co-authorship

The University of Tasmania (UTAS) allows the presentation of a thesis by incorporating published or submitted papers for the Degree of Doctor of Philosophy that have taken place during the period of candidature. This thesis consists of ten papers, of which eight of them have been peer reviewed and accepted and two are under review. Some of the publications have been modified to fit into the structure of the thesis. The bibliographical details of the work are outlined below, and the full publications of the peer-reviewed papers are in the Appendix submitted with this thesis.

The following people and institutions contributed to the publications as part of this thesis:

Seyedsadreddin Kianejadtejenaki, Australian Maritime College – University of Tasmania (AMC-UTAS)-(Candidate).

Dr. Hossein Enshaei, AMC-UTAS.

Dr. Jonathan Duffy, AMC-UTAS.

Prof. Dev Ranmuthugala, AMC-UTAS.

Ms Nazanin Ansarifard, AMC-UTAS.

Published papers:

PAPER 1, KIANEJAD, S., ENSHAEI, H. & RANMUTHUGALA, D. Estimation of added mass moment of inertia in roll motion through numerical simulation. PACIFIC 2017 International Maritime Conference, 2017. 1-15.

Located in chapter 3.

Candidate was the primary author while authors 2 and 3 assisted with refinement and presentation. [Candidate: 80%, Author 2: 15%, Author 3: 5%]

PAPER 2, S. S. KIANEJAD, H. ENSHAEI, J. DUFFY,N. ANSARIFARD, D. RANMUTHUGALA 2018a. Investigation of scale effects on roll damping through numerical simulations. Proceedings of the 32nd Symposium on Naval Hydrodynamics, Hamburge, Germany.

Located in chapter 4.

Candidate was the primary author and author 4 provided technical support in performing numerical simulations. While authors 2, 3 and 5 assisted with refinement and presentation. [Candidate: 76%, Author 2: 10%, Author 3: 6%, Author 4: 4%, Author 5: 4%]

PAPER 3, KIANEJAD, S., LEE, J., LIU, Y. & ENSHAEI, H. 2018. Numerical Assessment of Roll Motion Characteristics and Damping Coefficient of a Ship. Journal of Marine Science and Engineering, 6, 101.

Located in chapter 4.

Candidate was the primary author and with collaboration with authors 2 and 3 performed the numerical simulations. Author 4 assisted with refinement and presentation. [Candidate: 78%, Author 2: 8%, Author 3: 8%, Author 4: 6%]

PAPER 4, H. ENSHAEI, S. S. KIANEJAD. 2018b. Quantifying Ship's Dynamic Stability through Numerical Investigation of Weight Distribution. Proceedings of the 13th Int. Conference on the Stability of Ships and Ocean Vehicles (STAB), Kobe, Japan.

Located in chapter 2.

Author 1 was the primary author and conceived the idea while the candidate wrote the manuscript. [Candidate: 50%, Author 1: 50%]

PAPER 5, S. S. KIANEJAD, H. ENSHAEI, J. DUFFY,N. ANSARIFARD 2018c. Calculation of Restoring Moment in Ship roll motion through Numerical Simulation. Proceedings of the 13th Int. Conference on the Stability of Ships and Ocean Vehicles (STAB), Kobe, Japan.

Located in chapter 5.

Candidate was the primary author while Authors 2-4 assisted with refinement and presentation. [Candidate: 80%, Author 2: 10%, Author 3: 6%, Author 4: 4%]

PAPER 6, KIANEJAD, S. S., ENSHAEI, H., DUFFY, J., ANSARIFARD, N. & RANMUTHUGALA, D. 2019a. Ship Roll Damping Coefficient Prediction Using CFD. Journal of Ship Research.

Located in chapter 4.

Candidate was the primary author and author 4 provided technical support in performing numerical simulations. While authors 2, 3 and 5 assisted with refinement and presentation. [Candidate: 76%, Author 2: 10%, Author 3: 6%, Author 4: 4%, Author 5: 4%]

PAPER 7, KIANEJAD, S., ENSHAEI, H., DUFFY, J. & ANSARIFARD, N. 2019b. Prediction of a ship roll added mass moment of inertia using numerical simulation. Ocean Engineering, 173, 77-89.

Located in chapter 3.

Candidate was the primary author while authors 2-4 assisted with refinement and presentation. [Candidate: 80%, Author 2: 10%, Author 3: 6%, Author 4: 4%]

PAPER 8, KIANEJAD, S., ENSHAEI, H., DUFFY, J. & ANSARIFARD, N. 2019c. Investigation of a ship resonance through numerical simulation. Journal of Hydrodynamics, 1-15.

Located in chapter 2.

Candidate was the primary author while authors 2-4 assisted with refinement and presentation. [Candidate: 80%, Author 2: 10%, Author 3: 6%, Author 4: 4%]

Under review papers:

PAPER 9, KIANEJAD, S., ENSHAEI, H., DUFFY, J. Ship roll restoring moment calculation in beam sea condition. Ships and offshore structures (under review).

Located in chapter 6.

Candidate was the primary author while authors 2 and 3 assisted with refinement and presentation. [Candidate: 80%, Author 2: 10%, Author 3: 10%]

PAPER 10, KIANEJAD, S., ENSHAEI, H., DUFFY, J. Calculation of roll hydrodynamic coefficients in regular beam waves. Ocean Engineering (under review).

Located in chapter 7.

Candidate was the primary author while authors 2 and 3 assisted with refinement and presentation. [Candidate: 80%, Author 2: 10%, Author 3: 10%]

We the undersigned agree with the above stated "proportion of work undertaken" for each of the above published (or submitted) peer-reviewed manuscripts contributing to this thesis:

Signed:

Dr Hossein Enshaei
Supervisor
National Centre for Ports and Shipping
University of Tasmania

Date: 08/07/2019

Signed:

Dr Prashant Bhaskar
Director, National Centre for Ports & Shipping
Australian Maritime College
University of Tasmania

FOR: Mr Michael van Balen AO
Principal
Australian Maritime College
University of Tasmania

Date: 08/07/2019

Acknowledgement

Firstly, I thank the supervisory team (Dr. Hossein (Behrooz) Enshaei and Dr. Jonathan (Jon) Duffy) for their knowledge, support and patience. Their worthwhile advice enlightened the journey of PhD in my mind and helped me to gradually fade the unknowns and emerge spark of the knowledge. I would like to express my sincere gratitude to Behrooz and Jon for their valuable instructions, inspiration and encouragement benefiting my study. It has been greatly enjoyable to work together, and I could not have imagined having better supervisors and mentors for my thesis.

I thank Prof. Dev Ranmuthugala who was initially my supervisor for his insightful comments and support.

During the course of this work, I conducted model scale experiments using the towing tank facilities at the Australian Maritime College. I thank the team at the Towing Tank for their work in what was a challenging build. Your assistance made my time in the Towing Tank runs as smoothly as could possibly be hoped for.

I thank Nazanin Ansarifard for her support in discussing and solving the problems raised during the numerical and experimental simulations.

Very special gratitude goes out to all my friends down at the AMC Research Hub who have created a very memorable environment for research and celebrating life.

Finally, I thank my family for their on-going support in every situation and decision I have made in my life. My Parents who have done all they could for my happiness without expecting anything in return. My wife, Nazanin, who has always been inspiring and supporting during the hard moments and has been a true friend to me.

Abstract

Dynamic stability is the field of naval architecture, which analyses the stability of a ship and the onset of instability in encountering waves at sea. The study of dynamic stability aims to investigate the development of extreme roll motion and to find out if a ship is stable or unstable. This understanding leads to broad implications for the design and operation of ships and floating units. Researchers have an integrated notion of "ship stability, dynamics and safety" for investigating dynamic stability phenomena.

In practice, the intact stability for design and operation is evaluated through static conditions, which does not account for the effect of waves and winds at sea. This long-standing issue has been addressed by the second generation of intact stability criteria (SGISC) proposed by IMO in recent years, which defines a set of failure modes associated with potentially dangerous dynamic stability phenomena in waves. These phenomena are declared as parametric roll, pure loss of stability, surf-riding and broaching, dead ship condition and excessive acceleration.

Among those, roll resonance occurs because of two different phenomena of synchronous and parametric roll, where the encounter frequency is equal and two times the ship's natural roll frequency, respectively. The parametric roll is most probable to arise in some types of ships like containerships in a head sea condition when the wavelength is approximately equal to the ship's length. Whereas, all ship types may be subjected to the synchronous rolling in beam sea conditions. The roll resonance is a dangerous dynamic condition where a ship experiences an incremental roll angle, and in the worst scenario a large roll angle may capsize the ship. At the roll resonance condition, the magnitude of virtual roll moment of inertia is equal to the restoring moment but in the opposite direction, hence, they oppose each other and leave roll damping to resist the roll motion. Since the magnitude of roll damping is small for a typical ship, the external forces and moments induce a larger roll motion.

The investigation of parametric roll and dead ship condition using experiments and CFD simulations are expensive in terms of cost and time, whereas equation-based methods with a reasonable level of accuracy can be more effective in terms of expenses. Equation-based methods consist of the virtual roll moment of inertia (roll mass moment of inertia and roll added mass moment of inertia), damping and restoring moment coefficients. Therefore, this research aims to quantify those coefficients and their variations in different conditions. This study increases our understanding of the ship's dynamic stability by precisely calculating the roll hydrodynamic coefficients in calm water and regular beam sea conditions.

A numerical method is adopted and validated against experimental model tests to investigate the influence of several parameters on the magnitude of roll hydrodynamic coefficients in calm water condition including degrees of freedom (DOF), Froude number, excitation frequency, scale effect and appendages. In the second phase of the study, numerical and experimental simulations are conducted in regular beam sea conditions and a good correlation is found between the results. Furthermore, the effects of different wave heights and frequencies on the roll hydrodynamic coefficients in a beam sea condition are investigated.

This study introduces new methods of calculating the roll hydrodynamic coefficients including roll added mass moment of inertia, damping and restoring in calm water and regular beam sea conditions. These methods

can be generalised for application on other ship types to extract hydrodynamic coefficients applicable to equation-based methods for the precise prediction of ship motions. The findings are extremely useful for ship designers and researchers, which contribute in several ways to the understanding of ship stability and provide a basis for considering dynamic behaviours in the operational limitations.

Table of Contents

List of Figures

List of Tables

Chapter 1: Introduction

1.1 Background

Ship stability can be categorised into static and dynamic conditions. Fulfilling the criteria of static stability is compulsory for existing ships, while, ships in the real sea experience dynamic conditions and having satisfactory static stability does not guarantee the safety of ships. On the other hand, plenty of ships have good dynamic stability, whereas they are penalised from carrying enough cargo due to passing static stability criteria marginally.

Investigating the dynamic stability of ships in the intact condition is one of the popular research subjects in the field of naval architecture. Linear or weakly nonlinear approaches are probably accepted with a certain level of accuracy to investigate dynamic stability of ships; however, in the case of extreme sea conditions, which cause large amplitude motions (especially roll motion), a strong nonlinear approach is required.

To address this gap, in the recent years, the Second Generation of Intact Stability Criteria (SGISC) was proposed by IMO, which defines a specific set of failure modes associated with potentially dangerous dynamic stability phenomena in waves. Those phenomena are parametric roll, pure loss of stability, surf-riding and broaching, dead ship condition, and excessive accelerations. The failure modes are strongly nonlinear, and the relevant criteria for ensuring sufficient safety levels require the main specification of the underlying nonlinear dynamics. Hence, five aforementioned failure modes of SGISC give permission for incorporating methodologies at various steps of sophistication, starting from simple methods up to the utilisation of more intricate nonlinear ship motions.

A considerable number of papers have evaluated the dynamic of different failure modes and have represented feasible methodologies for addressing such failure at the design stage. However, the improvement by SGISC has expanded the ship stability evaluation to direct, semi-direct, and indirect approaches. With regard to SGISC, researchers are developing different approaches for the evolution of this framework to mitigate the hazard of these phenomena (Francescutto and Umeda, 2010, Umeda, 2013, Belenky et al., 2009). More progressive improvement of the situation has been achieved with regards to level 1 and level 2 of vulnerability criteria defined in SGISC for different failure modes. In this context, a number of researchers have considered time domain simulations for addressing parametric roll (Bulian et al., 2011, Peters et al., 2010), pure loss of stability (Peters et al., 2010), surf-riding and broaching (Umeda, 2013), dead-ship condition (Bulian et al., 2011), and excessive accelerations (Shigunov et al., 2011). In addition, sample estimations and conformity studies of accessible level 1 & 2 criteria have been performed. Several specific experimental simulations have been performed to verify the suggested numerical methods for being implemented in level 1 and level 2 criteria (Umeda et al., 2014). Special regard has been given to this topic using semi-direct approaches to assess dynamic stability to improve operational guidance; nevertheless, the interest is yet growing over time.

Roll resonance occurs in parametric roll and dead ship condition where a ship experiences larger roll angle under relatively smaller roll exciting moments. The focus of this study is to investigate the motion characteristics of a ship close to the resonance condition. Direct investigation (experimental and CFD simulations) of resonance is expensive in terms of cost and time, and equation-based methods have been utilised in most of the studies in this area. However, these methods cannot predict ships motions reasonably accurate unless their hydrodynamic

coefficients, including the added mass moment of inertia, damping and restoring moments are derived accurately. Accurate calculation of the hydrodynamic coefficients can also improve the simulation of ship motions. The influence of several parameters such as frequency, appendages, Froude number, degrees of freedom (DOF) and wave characteristics, which have direct effect on the magnitude of hydrodynamic coefficients are required to be investigated.

1.2 Research Questions

In order to have a better understanding of dynamic stability of ships at sea through equation-based method, it is imperative to estimate the roll hydrodynamic coefficients more accurately; hence the proposed work is broken down into a number of specific research questions as below:

- What are the effective parameters in calculating the roll hydrodynamic coefficients with a focus around resonance frequency?
- How to compute accurately the roll hydrodynamic coefficients of a model ship in calm water?
- How to compute accurately the roll hydrodynamic coefficients of a model ship in regular beam sea?

1.3 Research Aim and Objectives

The aim of this research is to improve the current state of scientific knowledge with regard to the dynamic stability of a ship. This is particularly to be addressed through the following objectives:

- To calculate the roll added mass moment of inertia more accurately in calm water and wave conditions.
- To calculate the roll damping more accurately in calm water and wave conditions.
- To calculate the roll restoring moment more accurately in calm water and wave conditions.
- To investigate the impact of degrees of freedom (DOF), Froude number, excitation frequency, scale effect, appendages, and wave characteristics on the roll hydrodynamic coefficients.

1.4 Novel aspects

While several original aspects have been developed in this study, the most outstanding outcomes that result from this work are deriving three distinguished hydrodynamic terms of roll motion equations:

- Calculating the restoring moment in the dynamic condition while considering the influential parameters in calm water and wave conditions.
- Calculating the added mass moment of inertia in calm water and wave conditions and specifying the influence of relevant parameters.
- Calculating the damping moment in calm water and wave conditions and specifying the influence of relevant parameters.

1.5 Significance of the study

There are different approaches to investigate the failure modes of dynamic stability (dead ship condition is the focus of this study) such as experimental measurements, numerical simulations and equation-based methods. The equation-based methods have been utilised in most studies to reduce the cost and time of the simulations. However, the validity of these methods depends on the accuracy of roll hydrodynamic coefficients. The most common methods for calculation of roll hydrodynamic coefficients fail to consider the impact of some parameters, hence, the magnitude of these coefficients remains inaccurate in some conditions. In this study, new approaches are presented for deriving these coefficients, including roll added mass moment of inertia, damping and restoring in the calm water and wave conditions. The effects of excitation frequency, appendages, Froude number, exciting moment, wave characteristics and scale effects on the magnitude of roll hydrodynamic coefficients are investigated.

The results of this research strengthen the idea that equation-based methods are suitable for ship motion predictions in ample time. The findings provide insights for designers and operators to precisely compute the hydrodynamic coefficients, which can improve the prediction of ship motions as well as investigation of dynamic stability. The proposed methods can be generalised to compute the roll hydrodynamic coefficients of other ship types.

1.6 Methodology

The precise calculation of added mass moment of inertia, damping moment and restoring moment is the main objective of this research. The first stage is a literature review, where related papers are studied to understand what other researchers have done and where the major questions remain. There are several approaches to compute the added mass moment of inertia, damping and restoring coefficients, but existing approaches can only be utilised in specific circumstances. Therefore, this study is focused on numerical and experimental tools to compute the roll hydrodynamic coefficients. For the numerical approach in this study, a CFD based software of STAR CCM+ is utilised, which solves the three-dimensional Reynolds-average Navier-Stokes equations with a complete turbulence model, based on a finite volume method.

In calm water condition, a model of a Post-Panamax container ship is excited based on harmonic excited roll motion technique, and the numerical results have been validated with an existing published experimental data, which established a set up for further simulations. The damping term is calculated by energy conservation method independently, and the roll added mass moment of inertia is calculated through a new method. Deducting the roll damping, mass and added mass moment of inertia terms from the total moment yields the residual moment, which would be the restoring moment. This innovative method uses sensitivity analysis to investigate the influence of effective parameters on roll motion characteristics. Upon establishing a valid numerical method to estimate the added mass moment of inertia, damping and restoring moments on a ship model, the method can be utilised for a full-scale ship. Although the Froude number of a ship and its model remains the same, their Reynolds' numbers are different, and the above-mentioned terms, and in particular the

damping is dependent on Reynold's number. This method can provide a more realistic prediction of a full-scale ship's behaviour in real sea condition.

In regular beam sea condition, a model of bulk carrier is excited by regular waves with different heights and frequencies. The motion characteristics from numerical simulations are then compared against experimental measurements, and a good correlation is found. The restoring and exciting moments in dynamic condition, considering the position of waves with respect to the model is calculated by numerical simulation. Following the successful quantification of restoring moments in waves, the roll damping and added mass moment of inertia are calculated using new approaches.

1.7 Organisation of thesis

Chapters 2 – 7 of this thesis are based on journal articles and conference papers prepared by the candidate. In the first page of each chapter, it is mentioned whether the paper is published or is under review by the journal. The chapter body is then the most recent version provided for publication (under review), some of the publications have been modified to fit into the structure of the thesis and all the published papers can be found in the appendix. An overview of the structure of this thesis is shown in Figure 1.1 and further details are provided below:

- ***Chapter 2: Roll Resonance in Calm Water (contains two papers)***

Paper 8: *KIANEJAD, S., ENSHAEI, H., DUFFY, J. & ANSARIFARD, N. 2019. Investigation of a ship resonance through numerical simulation. Journal of Hydrodynamics, 1-15.* This paper investigates the factors that influence the roll resonance to improve understanding of the resonance phenomenon using CFD simulation. Because, the calculation of roll hydrodynamic coefficients is performed at frequencies close to the natural frequency of the model. To achieve this aim, a container ship model was excited with a sinusoidal roll moment based on harmonic excited roll motion (HERM) technique over a range of frequencies, including those higher and lower than the roll natural frequency. In addition to the encounter frequency, the effects of phase shift between the roll exciting moment and roll angle, the phase difference between the roll angle and angular acceleration at resonance, are investigated.

Paper 4: *H. ENSHAEI, S. S. KIANEJAD. 2018. Quantifying Ship's Dynamic Stability through Numerical Investigation of Weight Distribution. Proceedings of the 13th Int. Conference on the Stability of Ships and Ocean Vehicles (STAB), Kobe, Japan.* In this study, the effects of different loading conditions and weight distributions on the roll motion characteristics are studied. A model of a post panamax container ship is excited at different excitation frequencies and Froude numbers to simulate the occurrence of roll resonance. Moreover, vertical centre of gravity (VCG) and roll moment of inertia as a result of weight distributions are also considered.

- ***Chapter 3: Roll added mass moment of inertia in calm water (contains two papers)***

Paper 7: *KIANEJAD, S., ENSHAEI, H., DUFFY, J. & ANSARIFARD, N. 2019. Prediction of a ship roll added mass moment of inertia using numerical simulation. Ocean Engineering, 173, 77-89.* In this study, the roll added

mass moment of inertia of a container ship is calculated by a new method. The model is excited by external sinusoidal roll moments based on the harmonic excited roll motion technique (HERM) at different excitation frequencies. The numerical method is validated against experimental simulations. Additionally, the effects of forward speed, appendages and scale effect on the roll added inertia coefficient are investigated. The magnitude of roll added mass moment of inertia of the proposed method is compared against Bhattacharyya's method.

Paper 1: *KIANEJAD, S., ENSHAEI, H. & RANMUTHUGALA, D. Estimation of added mass moment of inertia in roll motion through numerical simulation. PACIFIC 2017 International Maritime Conference, 2017. 1-15.* The former journal paper covers almost the content of this conference paper, so, this conference paper is placed in the appendix.

- ***Chapter 4: Roll damping calculation in calm water (contains three papers)***

Paper 6: *KIANEJAD, S. S., ENSHAEI, H., DUFFY, J., ANSARIFARD, N. & RANMUTHUGALA, D. 2019. Ship Roll Damping Coefficient Prediction Using CFD. Journal of Ship Research.* Numerical simulations are conducted to compute the roll damping coefficients considering energy conservation method based of HERM technique. The results of fully appended model free in 6 DOF are compared against experimental measurements and a good correlation is found. For the next stage, the impact of appendages, forward speed and DOF on the roll motion characteristics and roll damping coefficients for both model-scale and full-scale are investigated.

Paper 3: *S. S. KIANEJAD, H. E., J. DUFFY,N. ANSARIFARD, D. RANMUTHUGALA 2018. Investigation of scale effects on roll damping through numerical simulations. Proceedings of the 32nd Symposium on Naval Hydrodynamics, Hamburge, Germany.* The former journal paper coveres almost the content of this conference paper, so, this conference paper is placed in the appendix.

Paper 3: *KIANEJAD, S., LEE, J., LIU, Y. & ENSHAEI, H. 2018. Numerical Assessment of Roll Motion Characteristics and Damping Coefficient of a Ship. Journal of Marine Science and Engineering, 6, 101.* This paper investigates the effects of excitation frequency on roll damping coefficients based on HERM technique.

- ***Chapter 5: Roll restoring calculation in calm water (contains one paper)***

Paper 5: *S. S. KIANEJAD, H. E., J. DUFFY,N. ANSARIFARD 2018. Calculation of Restoring Moment in Ship roll motion through Numerical Simulation. Proceedings of the 13th Int. Conference on the Stability of Ships and Ocean Vehicles (STAB), Kobe, Japan.* In this study, a model of a container ship is excited to compute the restoring moment in dynamic condition using CFD simulations. Additionally, the effects of appendages, forward speed, and number of degrees of freedom (DOF) on the roll restoring moments at a frequency close to the natural frequency of the model are investigated. The restoring moment in dynamic condition for all conditions are compared agains restoring moment from hydrostatic calculations.

- ***Chapter 6: Roll restoring calculation in regular beam sea (contains one paper)***

Paper 9: *KIANEJAD, S., ENSHAEI, H., DUFFY, J. Ship roll restoring moment calculation in beam sea condition. Ships and offshore structures (under review).* In this study, the variation of restoring moment of a

model of bulk carrier ship in a dynamic condition is studied. The model is excited in 14 conditions in beam sea, including two wave heights of 0.05 and 0.1 m and seven frequencies close to the natural frequency of the model from 0.57 to 0.69 Hz with intervals of 0.02 Hz. The restoring moment is calculated considering the real amount of buoyancy force and position of the model with respect to the wave. The results in dynamic condition have significant differences compared with restoring moment in hydrostatic condition.

• ***Chapter 7: Roll added mass moment of inertia and damping calculations in regular beam sea (contains one paper)***

Paper 10: *KIANEJAD, S., ENSHAEI, H., DUFFY, J. Calculation of roll hydrodynamic coefficients in regular beam waves. Ocean Engineering (under review).* In this study, a model of bulk carrier ship is adopted to compute the magnitude of roll damping and added mass moment of inertia coefficients using experimental and numerical simulations. Novel methods are introduced for calculation of the roll damping and added mass moment of inertia coefficients. The model is excited in 35 cases in regular beam sea conditions, including five wave heights (0.025, 0.05, 0.075, 0.1 and 0.125 m) and seven frequencies, which are close to the natural frequency of the model from 0.57 to 0.69 Hz with intervals of .02 Hz.

• ***Chapter 8*** states the main conclusions and provides some ideas for further studies.

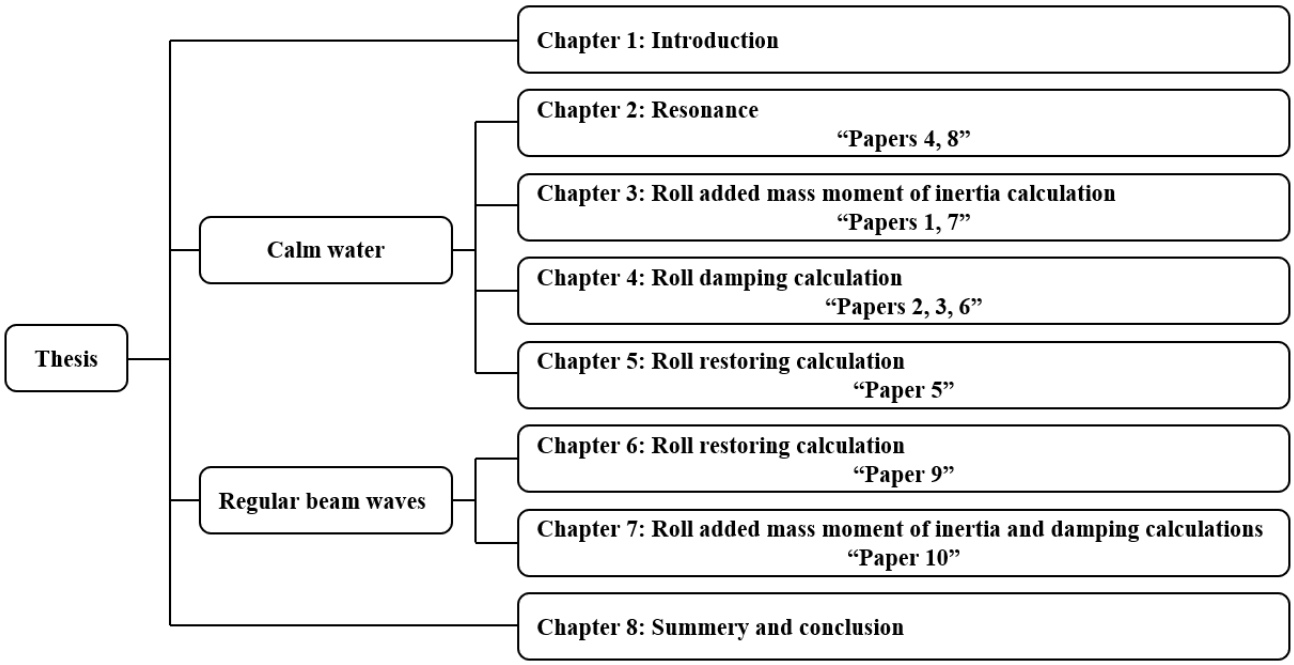

Figure 1.1 An overview of thesis chapters

Chapter 2: Roll Resonance in Calm Water

The works presented in this chapter have been published as peer reviewed papers. The citations for these papers are:

KIANEJAD, S., ENSHAEI, H., DUFFY, J. & ANSARIFARD, N. 2019c. Investigation of a ship resonance through numerical simulation. Journal of Hydrodynamics, 1-15.

H. ENSHAEI, S. S. KIANEJAD. 2018b. Quantifying Ship's Dynamic Stability through Numerical Investigation of Weight Distribution. Proceedings of the 13th Int. Conference on the Stability of Ships and Ocean Vehicles (STAB), Kobe, Japan.

Chapter 2 has been removed for copyright or proprietary reasons.

Chapter 3: Roll added mass moment of inertia calculation in calm water

The works presented in this chapter have been published as peer reviewed papers. The citations for these papers are:

KIANEJAD, S., ENSHAEI, H., DUFFY, J. & ANSARIFARD, N. 2019b. Prediction of a ship roll added mass moment of inertia using numerical simulation. Ocean Engineering, 173, 77-89.

KIANEJAD, S., ENSHAEI, H. & RANMUTHUGALA, D. Estimation of added mass moment of inertia in roll motion through numerical simulation. PACIFIC 2017 International Maritime Conference, 2017. 1-15.

Chapter 3 has been removed for copyright or proprietary reasons.

Chapter 4: Roll damping calculation in calm water

The works presented in this chapter have been published as peer reviewed papers. The citations for these papers are:

KIANEJAD, S. S., ENSHAEI, H., DUFFY, J., ANSARIFARD, N. & RANMUTHUGALA, D. 2019a. Ship Roll Damping Coefficient Prediction Using CFD. Journal of Ship Research.

S. S. KIANEJAD, H. ENSHAEI, J. DUFFY, N. ANSARIFARD, D. RANMUTHUGALA 2018a. Investigation of scale effects on roll damping through numerical simulations. Proceedings of the 32nd Symposium on Naval Hydrodynamics, Hamburge, Germany.

KIANEJAD, S., LEE, J., LIU, Y. & ENSHAEI, H. 2018. Numerical Assessment of Roll Motion Characteristics and Damping Coefficient of a Ship. Journal of Marine Science and Engineering, 6, 101.

Chapter 4 has been removed for copyright or proprietary reasons.

Chapter 5: Roll restoring moment calculation in calm water

The work presented in this chapter has been published as a peer reviewed paper. The citation for the paper is:

S. S. KIANEJAD, H. ENSHAEI, J. DUFFY,N. ANSARIFARD 2018c. Calculation of Restoring Moment in Ship roll motion through Numerical Simulation. Proceedings of the 13th Int. Conference on the Stability of Ships and Ocean Vehicles (STAB), Kobe, Japan.

Chapter 5 has been removed for copyright or proprietary reasons.

Chapter 6: Roll restoring moment calculation in regular beam waves

This chapter has been submitted for publication in journal of Ships and Offshore Structures, and at the time of writing the thesis was under review. The citation for the research article is:

KIANEJAD, S., ENSHAEI, H., DUFFY, J. (2019). Ship roll restoring moment calculation in beam sea condition. Ships and offshore structures (under review).

Abstract

Accurate calculation of restoring moment, virtual mass moment of inertia and damping moment increases the accuracy of a ship's dynamic stability simulation. The current methods of approximating the roll restoring moment are based on hydrostatic calculations. These methods fail to consider the dynamic conditions and variation of buoyancy and wave location with respect to the model. In the current study, experimental and numerical simulations are conducted at beam sea condition to investigate the behaviour of model. The model is excited by regular waves at different heights and frequencies to measure the motion characteristics and the restoring moment in dynamic conditions. The motion characteristics of the model obtained from the numerical simulation are compared against the experimental measurements, and a good agreement is found. The results show that the restoring moments in the dynamic condition have significant differences compared to the static condition. The magnitude of restoring moment in dynamic condition is measured based on the variation of heave motion of the model and the location of the wave's crest and trough with respect to the model.
Keywords: *Restoring moment, Buoyancy, CFD, Resonance, Beam waves.*

6.1 Introduction

A ship in the rough sea condition experiences nonlinear translational and rotational motions. However, there is a greater concern regarding roll motion compared to the other motions, as the damping and restoring moments which resist the roll motion increment, are smaller. As a result of the extreme roll, capsizing of a ship can occur both in resonance and non-resonance conditions (Wawrzyński and Krata, 2016). The non-resonance capsizing can occur in two different situations; when a ship experiences a large roll motion in a seaway which is also acted upon by gusty wind, and in surf-riding and broaching phenomena. On the other hand, the external forces and moments induced by waves at a specific frequency can excite the resonance condition. Capsizing in the resonance condition can occur due to two different phenomena of a synchronous and parametric roll, where the encounter frequency is either equal or two times of the ship's roll natural frequency, respectively. The parametric roll is most probable to arise in some types of ships like container ships in head sea condition when the wavelength is equal to the ship's length. Even though, all ship types might be subjected to the synchronous rolling in beam sea condition. This condition is dangerous since small external forces and moments can impose a large roll angle. To investigate a ship's motions, there are generally three approaches including experiments, CFD and equation-based methods. Direct investigation of different failure modes of dynamic stability is time-consuming; therefore, most studies have been conducted using equation-based methods. The accuracy of these methods depends on several hydrodynamic coefficients like the mass and added mass moment of inertia, damping and restoring. However, the magnitude and effects of restoring moment at a resonance condition are much larger than the other moments. Thus, computing the precise magnitude of the restoring part is imperative.

Paulling (1961) calculated the restoring moment in regular head sea condition using an analytical method. Neves and Rodríguez (2005) used a third order analytical model to compute the restoring moment based on an approach similar to Paulling. The weakness of this approach lies in the calculation of several geometry-based coefficients. Spyrou et al. (2008) utilized a panel code approach to calculate the restoring moment by reducing

the complexities of analytical methods. They found that the analytical method for a Matheiu type system cannot accurately capture the variation of righting arm in wave conditions.

Neves (2002), Neves et al. (2002) and Holden et al. (2007) used a 3 DOF nonlinear model to investigate the effects of heave, pitch and roll motions on the restoring moment. Although this model was simpler than 6 DOF, the computational time of the forces in the coupled motions was significant. Oh et al. (2000) suggested that modelling of the coupled heave, pitch and roll motions could be simplified since coupling effects on righting arm are small. They used a 1 DOF model by adding the coupled heave and pitch motions effects on the restoring moment, which was approximated by a third order fitting polynomial equation. In the case of regular waves, Bulian et al. (2006) introduced a 1.5 DOF model based on a quasi-static approach, where the half DOF is related to the coupled heave and pitch motions. They estimated the righting arm at different angles based on the height and position of the wave crest in relation to the ship's length using polynomial fitting function and Fourier series. In the case of irregular waves, they introduced Grim's effective wave (GEW) to estimate the righting moment which provides a conservative approximation. The GEW method was used by many researchers including Bulian (2008), Hashimoto (2006) and Umeda et al. (2004) in irregular wave condition. However, Somayajula and Falzarano (2017b) concluded that the results of the GEW model do not agree with a nonlinear time domain method which was validated against experiments. Bulian et al. (2008) also investigated the GEW method extensively and compared the results against experimental measurement, where the discrepancy was relatively high.

Palmquist (1994) and Hua et al. (1999) calculated the metacentric height in wave sea condition by a series of Volterra transfer functions. Somayajula et al. (2014) used this method to investigate the parametric roll of a container ship (C11) in head sea condition. The method failed to compute the restoring arm, while they calculated a time-variant cubic restoring arm in the next study (Somayajula and Falzarano, 2015). They concluded that both the Volterra approach and GEW overpredict the induced roll motion against experiments. Somayajula and Falzarano (2018) proposed a new model of the Volterra method (Volterra GZ method) to model the time-varying restoring arm in irregular waves without fitting approximation. The results were compared against a nonlinear time-domain method which had a better agreement.

Vidic-Perunovic (2011) and Dunwoody (1989) assumed a linear relationship between changes of metacentric height (GM) of a ship in the calm water and wave conditions based on the wave height. Silva et al. (2005) proposed that the restoring moment can be predicted accurately by computing the pressure distribution over the wetted surface area; however, this requires long-running simulations. They suggested a fifth-order nonlinear polynomial function instead of a direct calculation of the righting arm; although it is not feasible for some types of ships. Song et al. (2013) developed a 1 DOF method to predict the parametric roll that used a GM spectrum considering the coupled heave and pitch motions. The variation of the righting arm was estimated by combining the righting arm in the calm water and the fluctuation of the GM. The GM spectrum was computed considering the heave motion, pitch motion and wave elevation.

Hashimoto and Umeda (2004) reported that considering the dynamic component improves the prediction of restoring moment of a post panamax container ship. Bu et al. (2019) investigated the roll restoring arm variation

in both the head and following seas. They found that in head sea condition, the restoring arm has a nonlinear relationship with Froude number, while, the restoring arm is not sensitive to Froude number in the following sea condition. S. S. Kianejad (2018a) Calculated the dynamic restoring moment of a post panamax container ship in calm water condition based on a harmonic excited roll motion (HERM) method. They found that restoring moment in a dynamic condition is larger than restoring moment in static condition. They also noticed that equipping the model with bilge keels and considering the model free in higher DOF increases the restoring moment.

What is apparent from literature, a ship in the parametric roll and dead ship condition experiences the resonance condition where the roll angle increases over the time. The existing methods of predicting restoring moment of a ship fails to take into account the influence of dynamic condition, especially in the beam sea condition. The effect of buoyancy variation and position of a wave with respect to a ship are unknown. In this study, numerical and experimental simulations were conducted considering a beam sea condition at two wave heights (0.05 m and 0.1 m) and seven wave frequencies (from 0.57 to 0.69 Hz with intervals of .02 Hz) including lower and higher than the natural frequency of the model to investigate their influences on motion characteristics. The validated numerical method was used to calculate the roll restoring moment in a dynamic condition and investigate the effects of different wave heights and wave frequencies on it.

6.2 Model geometry

In this study, a model of bulk carrier ship is adopted to compute the magnitude of roll exciting and restoring moments as well as the roll damping and added mass moment of inertia coefficients. The main particulars of the model are shown in Table 6.1. The model had no appendages and was tested in regular beam sea conditions with no forward speed.

Table 6.1 Main particulars of the model

Main dimension	Model-scale
L_{pp} [m]	2.01
L_{wl} [m]	2.00
B_{wl} [m]	0.36
D [m]	0.09
C_B	0.81
Δ [Kg]	55.38
KG [m]	0.14
T_0 [s]	1.54
I_{xx} [Kg.m^2]	0.76
I_{yy} [Kg.m^2]	13.63
I_{zz} [Kg.m^2]	13.63

6.3 Experimental measurements

The model tests were conducted in the towing tank with 100 m length, 3.55 m width and a variable depth up to 1.5 m at the Australian Maritime College, University of Tasmania. A hydraulically driven wave maker located at one end of the towing tank was used to produce regular waves. A computer program was used to control the wave maker paddle to produce a range of waves with different heights and frequencies. A large beach is placed at the other end of towing tank to minimise the wave reflections. Figure 6.1 illustrates the model position in the

towing tank in a beam sea condition at an encounter angle of 90 degrees to the regular waves. To monitor the wave height and wave frequency of the produced waves, four resistive-type wave probes (named as WP0-WP3) were utilised. An optical motion tracking system (Qualisys) with seven cameras was employed to capture the translational and rotational motions of the model, as well as the roll angular velocity and roll angular acceleration. The centre of gravity of the model was set as a reference for the motion characteristics calculation via three passive markers attached to the model. It can be seen in Figure 6.1, the model was restrained by cables to decrease the sway and yaw motions. The cables were attached to the bow and stern of the model at the free surface to reduce their impacts on heave and pitch motions. The cables were threaded through pulleys at both sides of the tank and were restrained by 1 kg weights. All devices were synchronised, and the data was captured at 200 Hz for both the wave probes and Qualisys system.

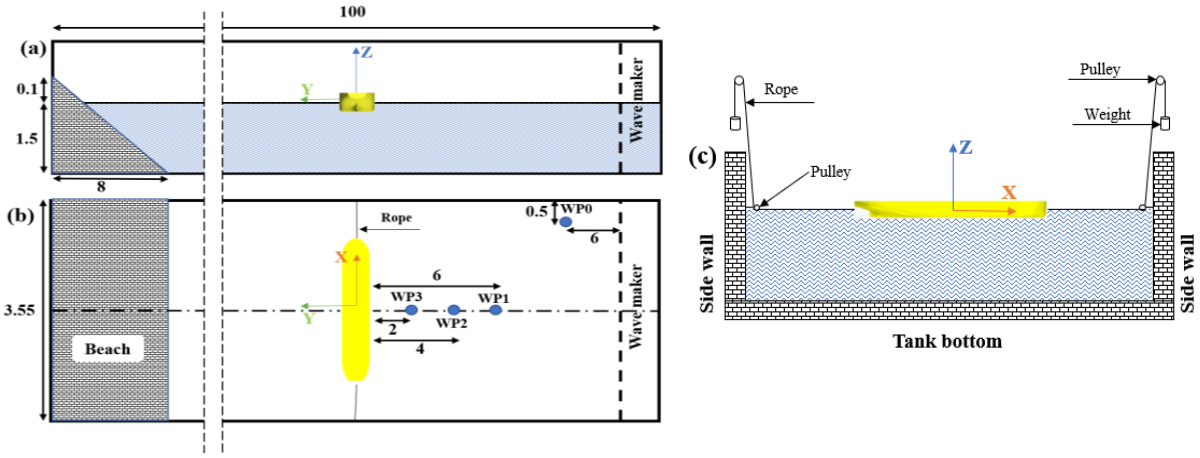

Figure 6.1 Experiment layout at different views in the towing tank (Dimensions are in meter).

6.4 Numerical modelling

The following sections discuss the details of numerical simulation method selected for this study.

6.4.1 Governing equations and physics modelling

The numerical simulations were carried out using STAR CCM+. The software resolves integral forms of RANS equations based on the finite volume method and a transient approach was selected as the simulation is a function of time. The solver utilises the averaged continuity and momentum equations. The aforementioned equations for incompressible flow in terms of tensor form and Cartesian coordinates are as follows (Ferziger et al., 1997):

$$\nabla.\mathrm{u} = 0 \tag{6.1}$$

$$\frac{\partial \rho \mathrm{u}}{\partial t} + \nabla.[\rho \mathrm{uu}] = -\nabla p^{*} + \mathrm{g.x}\nabla\rho + \nabla.[\mu\nabla \mathrm{u} + \rho\tau] \tag{6.2}$$

Here, X=(x, y, z) are the cartesian coordinates and u=(u, v, w) represent time averaged velocity fields and ∇ is the gradient operator. ρ is the density of water and air with a constant value for each one during the simulations. *P** and g represent the time averaged pressure and gravitational acceleration, respectively. τ and μ are the Reynolds tensor and the dynamic viscosity. A predictor-corrector method is employed to make a

correlation between continuity and momentum equations. The turbulence models are required to provide closure of the RANS equations in a turbulent flow and to address the uncertainty of the stress tensor, hence, the SST and K-omega turbulence model was selected.

The "volume of fluid" (VOF) approach has been used for modelling of the free surface, which is a simple multiphase approach. While a VOF method is selected, there is no need for extra modelling. This is because VOF can be utilised for simulating flows with different phases in which each phase has a large structure with a low contact area with other phases. The free surface in calm water and wave condition changes during the simulation so that the second-order convection scheme was selected to capture a sharp interface among phases. The volume of fraction (γ) was utilised to track the fluids. The magnitude of volume of fraction for the air and water phases is 0 and 1, respectively, and a mixture of two fluids has an intermediate value. The volume fraction distribution is modelled by the equations below:

$$\frac{\partial \gamma}{\partial t} + \nabla.[\mathrm{u}\gamma] + \nabla.[\mathrm{u_r}\gamma(1-\gamma)] = 0 \tag{6.3}$$

The last term of equation 6.3 is a compression term which reduces the smearing of interface and u_r is the relative velocity. The variation of ρ and μ can be calculated by:

$$\rho = \gamma\rho_{water} + (1+\gamma)\rho_{air} \tag{6.4}$$

$$\mu = \gamma\mu_{water} + (1+\gamma)\mu_{air} \tag{6.5}$$

The solver utilises the segregated flow model to solve the governing equations in an uncoupled condition, where convection terms were discretised by the second order upwind scheme and the SIMPLE algorithm was selected throughout the solution. The model was free in 6 DOF to simulate the ship's motion like a real condition at sea. Thus, the dynamic fluid body interaction (DFBI) approach was used to feed the solver to compute different forces and moments, which are acting on the model. Courant number (CFL) was utilised to choose a suitable time step and it was less than one for each cell to have numerical stability. The force from the waves in y direction is large enough, the model experiences the sway motion. Therefore, four 10 N forces were applied on the model as shown in Figure 6.2 at the free surface to reduce the sway and yaw motions. When the model has the positive or negative sway motions, the forces with red and green forces, respectively, act on the model to bring it back to the initial sway position. As the simulations were set in beam sea condition with long crested regular waves and the moments generated by restraining forces were not considered, the yaw and pitch motions are negligible. The motions of the model are studied in section 6.7.1.

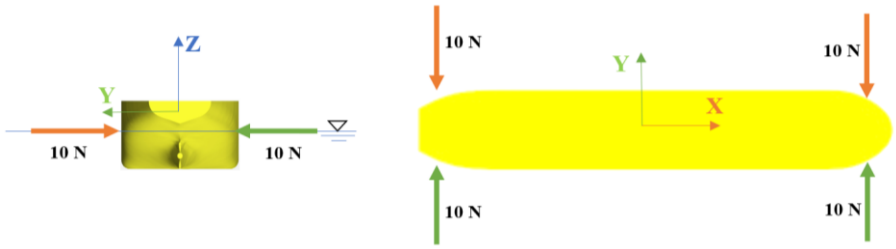

Figure 6.2 A schematic diagram of restraining the model in the numerical simulations.

6.4.2 Mesh structure and generation

Selecting a suitable size of the domain reduces the simulation time and increases the accuracy of the results. In this study, the domain size was selected based on practical guidelines for ship CFD applications proposed by ITTC (2011) where the inlet boundary is placed at 2.5 Lpp upstream of the model, while the outlet is placed at 4 Lpp downstream of the model. The top and bottom boundaries are located at 0.5 Lpp and 1 Lpp from the model, respectively, to avoid boundary effects on the simulation results. The side boundaries are positioned at 0.4 Lpp from the model. In order to capture large motions, the overset mesh approach was employed. This approach consists of two regions including overset and background. The overset region surrounds and holds the body and moves with the body inside the motionless background mesh (Field, 2013). The size of mesh inside the overset region was refined enough to capture the boundary layer, flow separation during body motion, wave making and vortices around the body. Four types of meshers were used to produce the mesh including trimmed, prism layer, surface and automatic surface repair meshers. The trimmed mesher creates a high-quality mesh, while the prism layer mesh was utilised to generate orthogonal prismatic mesh next to the body to capture the velocity gradient and boundary layer. To enhance the quality of surface to create volume mesh, the surface remesher was used. Finally, the automatic surface repair was used to refine the geometry problems that remained after surface remeshing. The size of cells inside the overset region is smaller than in the background region. To prevent divergence, the cell size in the overset region and the background were matched using an overlap volumetric block. The mesh at free surface was generated based on practical guidelines for ship CFD applications (ITTC, 2011). According to these recommendations for regular wave conditions, at least 40 cells per wavelength and 20 cells for the vertical direction of free surface were considered. The size of cells around the model was decreased to 40% of the basic cell size of the overset region and 15 inflation layers were generated by a stretching ratio of 1.3 using prism layer mesher to capture the boundary layer and flow separation around the body. The all y^+wall treatment was used which is a hybrid method and emulates the low y^+ wall treatment ($y^+ \sim 1$) for fine meshes and a high y^+ wall treatment for coarse meshes. The y+ value is less than 1 to ensure the selected mesh configuration has ability to compute the pressure and shear forces precisely. Figure 6.3 shows illustrations of the computation mesh. Details on the mesh sensitivity and uncertainty are provided in Section 6.6.

6.4.3 Boundary and initial conditions

To reduce the running time and boost the accuracy of simulation results, suitable initial and boundary conditions were selected. The velocity inlet boundary condition was set in upstream (inlet) of the model, while the pressure outlet boundary was set in downstream (outlet) to prevent any backflow. The top and bottom were set as velocity inlet, while, the side walls were set as a wall like the model tests. The magnitude of initial and boundary flow velocity at each velocity inlet boundary condition was set as fifth order wave condition. The initial hydrostatic pressure of the fifth order wave was set for the outlet boundary. For the lager wave heights, the wave profile in crest and trough is different and usually has sharper crest and wider trough. The fifth order Stokes wave produces more realistic regular waves like the obtained for the model tests, hence, the fifth order

waves were generated in this study. The VOF wave forcing method was selected at inlet and outlet boundaries to decrease the simulation time without compromising the results. The solution of 3D Navier Stokes equations at forcing length region (one wave length from each boundary) is forced towards a simplified theory (such as a theoretical solution or simplified numerical solution), where the momentum sources are used not phase and turbulence sources. As the 3D Navier Stokes equations are solving just at the vicinity of the model, the simulation time decreases. By setting the VOF wave forcing method at the inlet and outlet boundaries, propagating waves at the upstream decreases and better waves are produced.

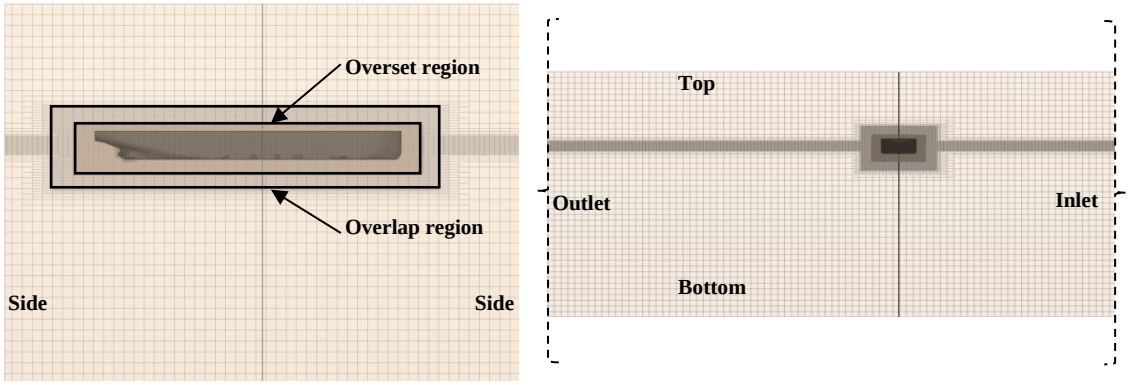

Figure 6.3 An overview of computational mesh and boundaries.

6.5 Experimental uncertainty

According to Kim and Hermansky (2014), the uncertainty of experimental measurements should be quantified to assess the quality of results. The experimental uncertainty consists of type A and type B based on the ISO-GUM's method. The type A uncertainty is based on the repeatability of measurements and is manifested in experimental variance:

$$s^2(q_k) = \frac{1}{n-1}\sum_{j=1}^{n}(q_j - \bar{q})^2 \tag{6.6}$$

Where, n is the number of repeated realizations and q_j is the value from a single measurement, $\bar{q}$ represents the mean value of the measured data. The experimental standard deviation is defined as a positive square root of variance. The standard type A uncertainty of a repeated measurement is computed by the equation below:

$$s(\bar{q}) = \frac{s(q_k)}{\sqrt{n}} \tag{6.7}$$

The end to end multiple test run approach is a common approach of the repeatability of measurement. In this regard, all influential parameters on measurement should be taken into account. To reduce the magnitude of type A uncertainty, the number of repeats should be large enough, and generally 10 repeats are acceptable. As the computation of uncertainty for all realizations is time consuming and costly, uncertainty calculation for a couple of realizations is suitable; hence, the repeats should be carefully selected. The type B uncertainty is defined by u_i^2 and/or u_i, which could be specified based on the variance and standard deviation. The geometry of model, measuring devices, calibration and installation of devices, data processing and presenting are the main sources of the type B uncertainty. The accuracy of Qualisys system and wave probe as measuring devices was chosen as sources of the type B uncertainty and remains constant over the duration of an experiment. The total

standard uncertainty of a measured value containing the type A and type B uncertainties can be computed by the equation below:

$$u(y) = [\sum_{i=1}^{N} s^2(\bar{q}) + \sum_{j=1}^{K} u^2(x)]^{1/2} \quad (6.8)$$

In the present study, the uncertainty calculation was conducted in cases with a wave height of 0.1 m and different frequencies as shown in Table 6.2 and Table 6.3. The total standard uncertainty at a wave frequency of 0.57 Hz is larger than the other cases, however, at frequencies closer to the natural frequency of the model (0.65 and 0.67 Hz) the uncertainty values are smaller. This is because, the motion characteristics variations for different repeats at resonance condition are negligible.

Table 6.2 Type A and B uncertainties of the experimental measurements at a wave height of 0.1 m and different wave frequencies.

Amplitude	**Type A Uncertainty**							**Type B Uncertainty**
Frequency (Hz)	0.57	0.59	0.61	0.63	0.65	0.67	0.69	
Roll angle (Degrees)	0.18	0.17	0.15	0.14	0.13	0.13	0.14	0.473
Angular velocity (Rad/s)	0.051	0.038	0.036	0.028	0.027	0.031	0.032	0.008
Angular acceleration (Rad/s^2)	0.179	0.174	0.164	0.159	0.151	0.152	0.158	0.008
Wave elevation (mm)	1.01	1.00	1.24	1.11	1.02	1.05	1.08	0.2
Heave (mm)	1.82	1.56	1.32	1.23	1.14	1.35	1.47	1.5
Sway (mm)	3.92	3.17	2.87	2.15	1.71	1.85	2.61	1.5

Table 6.3 Total standard uncertainty of the experimental measurements at a wave height of 0.1 m and different wave frequencies.

Amplitude	**Standard uncertainty (%)**						
Frequency (Hz)	0.57	0.59	0.61	0.63	0.65	0.67	0.69
Roll angle (Degrees)	4.17	3.54	3.04	2.74	2.65	2.64	2.69
Angular velocity (Rad/s)	6.22	4.11	3.32	2.37	2.18	2.22	2.39
Angular acceleration (Rad/s^2)	5.76	4.27	3.550	3.448	2.928	2.585	2.676
Wave elevation (mm)	2.02	2.01	2.42	2.16	2.04	2.05	2.14
Heave (mm)	4.95	4.29	3.82	3.62	3.48	3.64	3.79
Sway (mm)	8.84	7.17	6.48	5.13	4.32	4.76	6.05

6.6 Numerical uncertainty analysis

Prior to commencing the simulations for different cases, it is necessary to specify the uncertainty in simulation results to ensure the numerical approach simulates the physics accurately. According to the verification method advised by Stern et al. (2001), numerical uncertainty (U_{SN}) consists of iterative convergence uncertainty (U_I), grid-spacing uncertainty (U_G) and time-step uncertainty (U_T) given in the following equation:

$$U^2_{SN} = U^2_I + U^2_G + U^2_T \quad (6.9)$$

The uncertainty of the U_I is negligible for the fine grid and small time step (Tezdogan et al., 2015). The grid-spacing and time step were considered as major sources of the numerical uncertainties. To compute the numerical uncertainty, the simulation at a wave height of 0.1 m and a frequency of 0.65 Hz was selected. The grid-spacing uncertainty of different mesh configurations was performed based on a Richardson extrapolation (Kianejad et al., 2018). Three different mesh configurations with a refinement ratio of $r_G = \sqrt{2}$ were considered, and the number of meshes for each case is shown in Table 6.4. The simulation was set on the basis of coarse, medium and fine mesh configurations shown by S_3, S_2 and S_1, respectively. The variation of simulation results is calculated by the following equations:

$$\varepsilon_{G32} = S_3 - S_2 \tag{6.10}$$

$$\varepsilon_{G21} = S_2 - S_1 \tag{6.11}$$

$$R_G = \varepsilon_{G21} / \varepsilon_{G32} \tag{6.12}$$

Table 6.4 The number of elements for each mesh configuration tested.

	Background	**Overset**	**Total**
Fine (S_1)	525,546	2,040,984	2,566,530
Medium (S_2)	308,270	1,209,775	1,518,045
Coarse (S_3)	189,897	854,423	1,044,320

The numerical convergence ratio was calculated using equation 6.12. According to the convergence ratio, four typical conditions can be predicted: (i) monotonic convergence ($0<R_G<1$), (ii) oscillatory convergence ($R_G<0$; $|R_G|<1$), (iii) monotonic divergence ($R_G>1$), and (iv) oscillatory divergence ($R_G<0$; $|R_G|>1$). Numerical uncertainty in cases (iii) and (iv) cannot be computed because of divergence. For case (ii) uncertainty can be computed based on bounding error with upper limit S_U and lower limit S_L by using the equation below:

$$U_G = \left|\frac{1}{2}(S_U - S_L)\right| \tag{6.13}$$

In case (i), the generalised Richardson extrapolation should be adopted to compute the numerical error $\delta^*_{RE_{G1}}$ and order of accuracy P_G as shown in the equations below:

$$\delta^*_{RE_{G1}} = \frac{\varepsilon_{G21}}{r_G^{p_G} - 1} \tag{6.14}$$

$$p_G = \frac{\ln(\varepsilon_{G32} / \varepsilon_{G21})}{\ln(r_G)} \tag{6.15}$$

The correction factor C_G, which is defined in the equation below, determines the method of uncertainty calculation.

$$C_G = \frac{r_G^{p_G} - 1}{r_G^{p_{Gest}} - 1} \tag{6.16}$$

If the C_G is close to 1, the solutions are close to the asymptotic range and the numerical error δ^*_{SN}, benchmark result S_C and uncertainty U_{GC} can be computed from the following set of equations (Stern et al., 2006):

$$\delta^*_{SN} = C_G \times \delta^*_{RE_{G1}} \tag{6.17}$$

$$S_C = S - \delta^*_{SN} \tag{6.18}$$

$$U_{GC} = \begin{Bmatrix} (2.4(1-C_G)^2 + 0.1)\,|\,\delta^*_{RE_{G1}}\,| & \leftrightarrow |1-C_G| < 0.125 \\ |1-C_G\,|\,\delta^*_{RE_{G1}}\,| & \leftrightarrow |1-C_G| \geq 0.125 \end{Bmatrix} \quad (6.19)$$

If the value of C_G is greater than 1, the solutions are far from the asymptotic range and the numerical uncertainty should be computed by:

$$U_G = \begin{Bmatrix} (9.6(1-C_G)^2 + 1.1)\,|\,\delta^*_{RE_{G1}}\,| & \leftrightarrow |1-C_G| < 0.125 \\ (2\,|1-C_G\,| + 1)\,|\,\delta^*_{RE_{G1}}\,| & \leftrightarrow |1-C_G| \geq 0.125 \end{Bmatrix} \quad (6.20)$$

The time step uncertainty calculation was performed in a similar procedure and starting from $\Delta t = T/2^8$ and considering a refinement ratio of 2 (r_T=2). The numerical simulation results for each mesh configuration and time step, experimental measurements and the magnitude of uncertainties are presented in Table 6.5 and Table 6.6. Figure 6.4 shows the time traces of simulation results against experimental measurements and it can be seen that there is a good correlation between them. The magnitude of grid spacing uncertainty is larger than the time step uncertainty, accounting for 5% of maximum uncertainty for the sway motion. The simulation results for the fine mesh configuration and the smallest time step were closer to the experiment, hence, further simulations were performed based on the fine mesh configuration and smallest time step. The validation uncertainty (U_υ) can be calculated by equation 6.21, where, U_D is the experimental uncertainty. The absolute comparison error (E) is the difference between the numerical and experimental measurements. The absolute comparison error should be less than the validation uncertainty to validate the simulation results against experimental measurements.

$$U_\upsilon = \sqrt{U_{SN}^2 + U_D^2} \quad (6.21)$$

It can be seen in Table 6.7 that the magnitude of validation uncertainty for all cases is larger than the magnitude of absolute error and therefore, validation is confirmed.

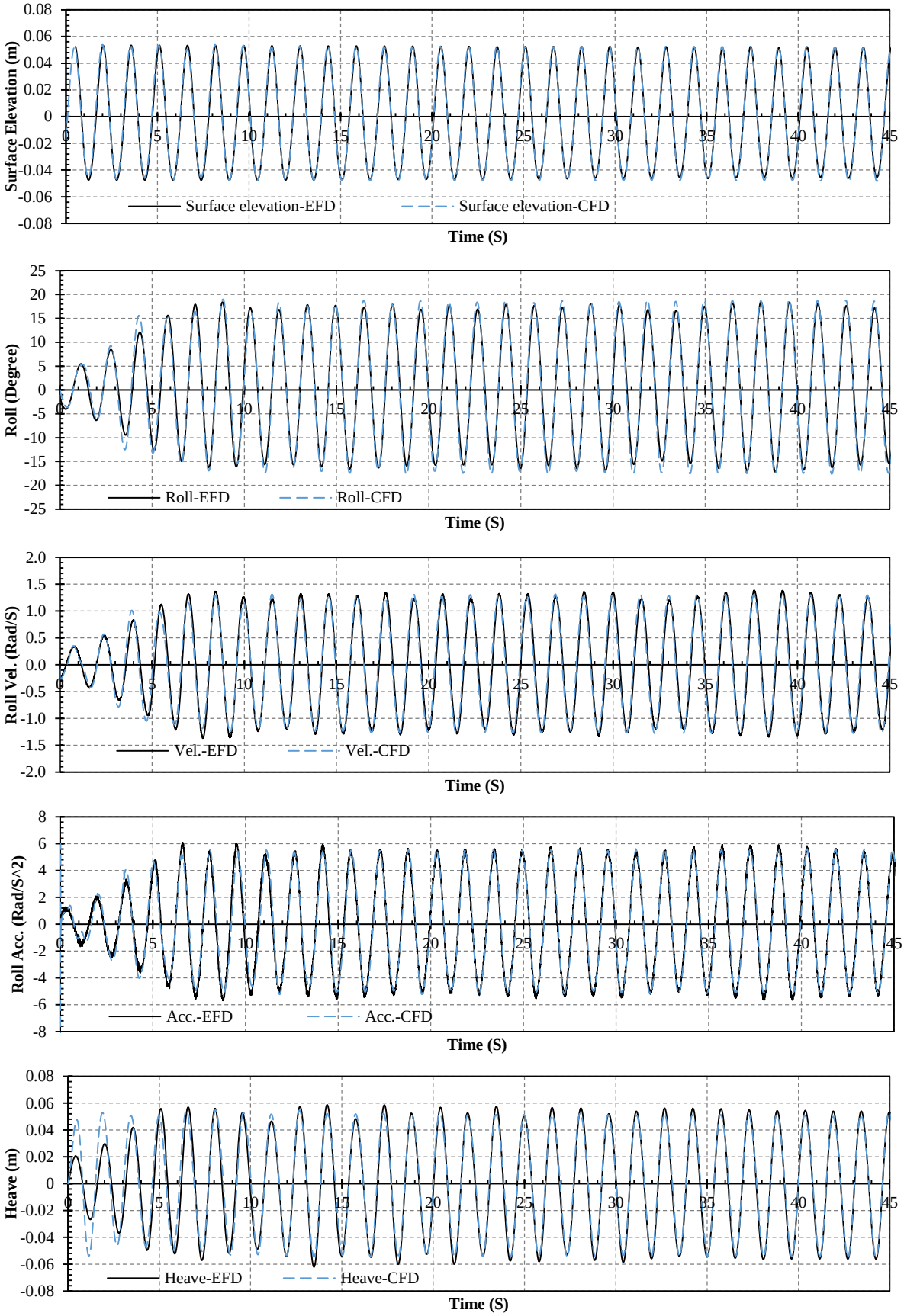

Figure 6.4 Surface elevation, roll angle, roll angular velocity, roll angular acceleration and heave motion time traces for the experimental and numerical simulations at a wave height of 0.1 m and a wave frequency of 0.65 Hz.

Table 6.5 Grid convergence study at a wave height of 0.1 m and a wave frequency of 0.65 Hz.

Amplitude	EFD	S_1	S_2	S_3	R_G	$\delta^*_{REG1}(\%S_1)$	$U_{GC}(\%S_1)$
Roll angle (Degrees)	18.51	18.80	19.00	19.41	0.49	1.01	1.76
Angular velocity (Rad/s)	1.3	1.26	1.29	1.34	0.60	3.57	4.37
Angular acceleration (Rad/s^2)	5.15	5.01	5.07	5.17	0.60	1.80	2.20
Wave elevation (mm)	51.02	50.18	49.41	48.45	0.67	2.40	2.40
Heave (mm)	54.13	52.42	51.34	48.84	0.44	1.65	3.35
Sway (mm)	52.67	56.11	54.46	52.18	0.63	4.46	5.05

Table 6.6 Time step convergence study at a wave height of 0.1 m and a wave frequency of 0.65 Hz.

Amplitude	EFD	T_1	T_2	T_3	R_T	$\delta^*_{RET1}(\%T_1)$	$U_{TC}(\%T_1)$
Roll angle (Degrees)	18.51	18.80	18.30	17.53	0.65	4.93	1.13
Angular velocity (Rad/s)	1.3	1.26	1.19	1.08	0.64	9.72	2.08
Angular acceleration (Rad/s^2)	5.15	5.11	5.023	4.91	0.82	7.93	3.08
Wave elevation (mm)	51.02	50.18	49.24	48.12	0.73	4.27	1.33
Heave (mm)	54.13	52.42	51.03	48.68	0.61	4.16	0.74
Sway (mm)	52.67	56.11	54.45	52.09	0.67	5.70	1.43

Table 6.7 Validation of the numerical simulation

	$U_{SN}(\%)$	$U_D(\%)$	$U\upsilon(\%)$	E (%)
Roll angle (Degrees)	2.09	2.65	3.38	-1.57
Angular velocity (Rad/s)	4.84	2.18	5.30	3.08
Angular acceleration (Rad/s^2)	3.78	2.93	4.78	2.72
Wave elevation (mm)	2.75	2.04	3.42	1.96
Heave (mm)	3.43	3.48	4.88	3.14
Sway (mm)	5.25	4.32	6.79	-6.45

The case of 0.1 m wave height and a wave frequency of 0.65 Hz was chosen to investigate the influence of turbulence model and side wall effects on the simulation results, and to ensure the reliability of the selected numerical approach. The simulations results are shown in Table 6.8. The simulations were performed by a cluster with 140 CPUs and the simulation time of the K-epsilon turbulence model (19 hours) was lower than the SST and K-omega turbulence model (24 hours), whereas, the simulation results had larger discrepancies compared to the experimental measurements. As the SST and K omega turbulence model generates more accurate results, it was chosen for the rest of simulations.

To investigate the effects of side walls on simulation results, both walls were positioned at 1.5 L from the model. The numerical set up was the same for the original and new wall positions. The simulation results in Table 6.8 and Figure 6.5 confirm that the wall effects are negligible. Since the simulations were conducted in beam sea condition and the width of the model is relatively small and the interaction between fluid and walls has a negligible impact on the model responses, hence, the original position of the side walls was considered for the rest of simulations to reduce the simulation time.

Table 6.8 Influence of turbulence model and side wall-effect on the simulation results.

	Original wall position			Wall-away
Amplitude	EFD	SST K-omega	K-epsilon	SST K omega
Roll angle (Degrees)	18.51	18.80	20.41	18.76
Angular velocity (Rad/s)	1.3	1.26	1.41	1.28
Angular acceleration (Rad/s2)	5.15	5.11	5.83	4.98
Wave elevation (mm)	51.02	50.18	50.23	50.15
Heave (mm)	54.13	52.42	50.24	53.04
Sway (mm)	52.67	56.11	54.83	55.52

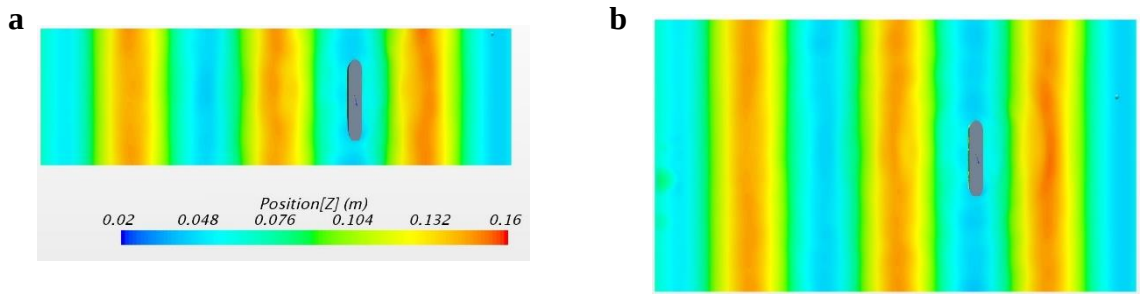

Figure 6.5 Investigation of side wall-effects of on wave profile, a) original wall location, b) side walls located at 1.5L from the model

6.7 Results and discussion

In this section, the results of motion characteristics of the model are presented for comparison and further discussion at different wave heights and wave frequencies for both numerical and experimental simulations. Additionally, for the roll angle amplitude, the results of static condition (from Maxsurf Stability version 20) are demonstrated to be compared against the dynamic condition. The magnitude of restoring moment at different conditions are also calculated and compared against the equivalent hydrostatic conditions. In the following sections, the model is located in the crest and trough conditions reflect that the model is located in zones 1 and 2, respectively (Figure 6.6).

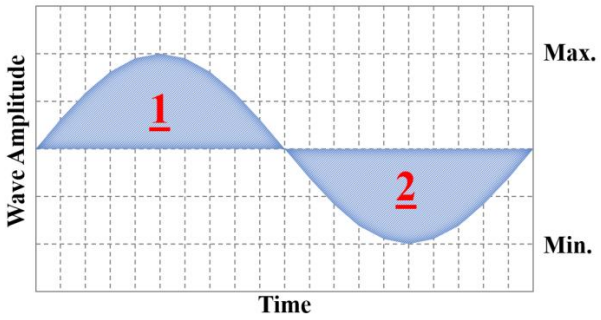

Figure 6.6 Zones for the crest (1) and trough (2) conditions.

6.7.1 Motion characteristics

The impact of two wave heights and seven wave frequencies were investigated on the responses of the model in the beam sea. The amplitude of roll angle, roll angular velocity, roll angular acceleration and heave motion are plotted in Figure 6.7. It can be seen that the results of numerical simulations are in a good agreement with the experimental measurements. Two figures are given for each one of the motion characteristics, one for a condition that the model is located in the trough of a wave (left figures), and the other when hit by the crest (right figures). The roll angle amplitudes in the dynamic condition (CFD and EFD) are also compared against static condition using hydrostatic calculation. In the static condition, the model was located at different locations of one wavelength (see Figure 6.8). The roll angle was calculated by computing the restoring moment and considering the variation of the restoring moment for various roll angles in a calm water condition. For the static condition, the roll amplitude increases linearly by increasing the wave frequency and wave height, because both of them increase the wave steepness, righting arm and restoring moment. Whereas, in the dynamic condition, especially at a wave height of 0.05 m, the roll amplitude increases by increasing the wave frequency to push the

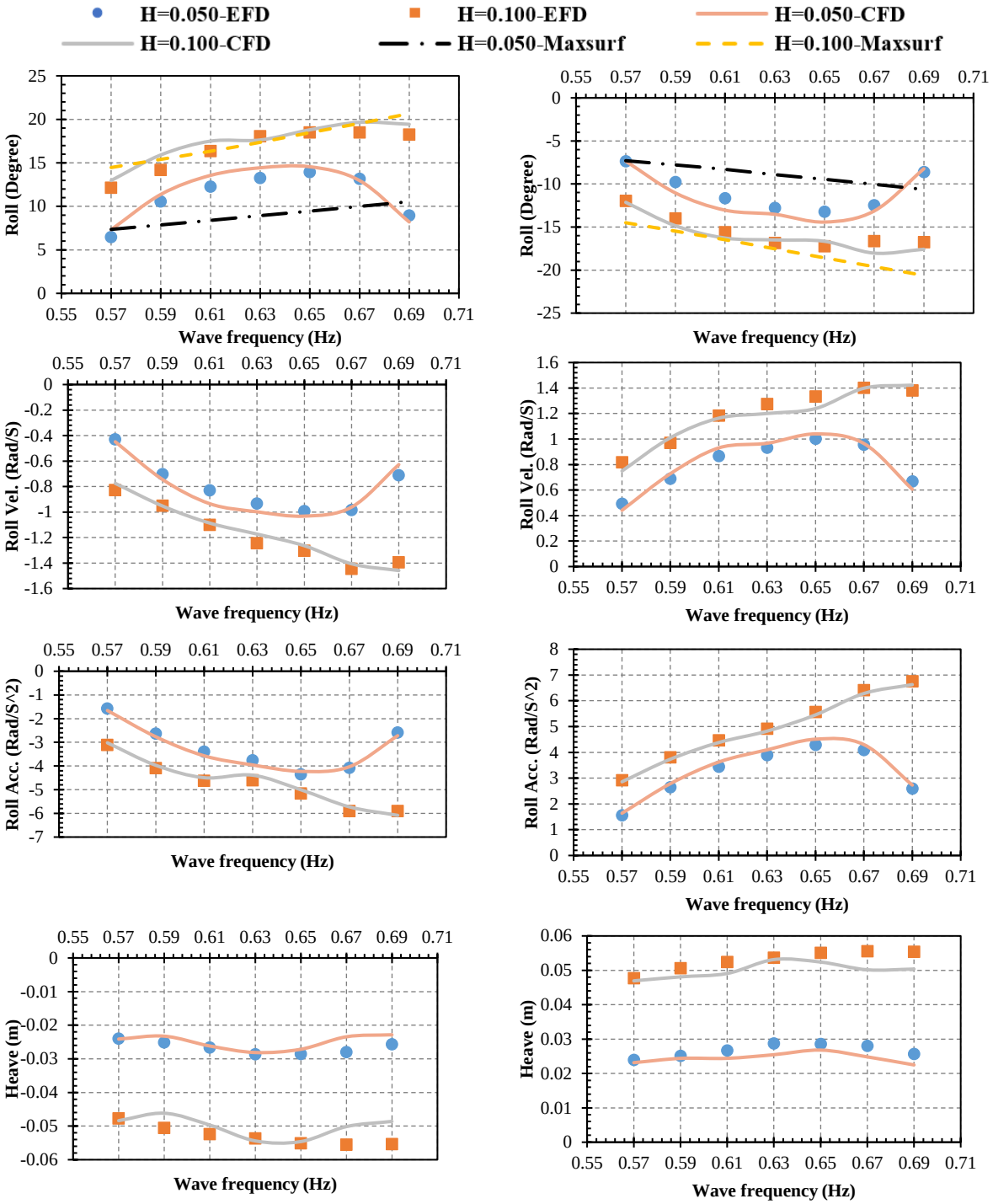

Figure 6.7 Amplitude of roll angle, roll angular velocity, roll angular acceleration and heave motion of the experimental and numerical simulations for the wave heights 0.05 and 0.1 m at wave frequencies of 0.57 to 0.69 Hz.

roll angle to the maximum value at the wave frequency of 0.65 Hz, which is close to the natural frequency of the model. After that, the roll angle decreases while wave frequency increases. However, the natural frequency of the model changes in the larger roll angles and wave heights (Kianejad et al., 2019b, H. Enshaei, 2018) and shifts the natural frequency towards a higher frequency, and as a result, the model experiences a larger roll angle at the wave frequency of 0.67 Hz. The roll angular velocity and acceleration follow the same patterns as the roll angle. They also have larger magnitudes close to the natural frequency of the model. It is apparent that

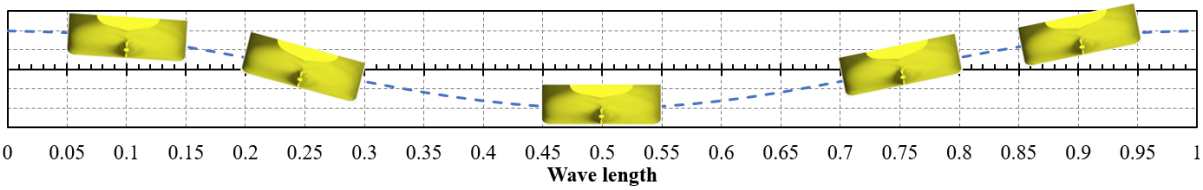

Figure 6.8 Positioning of the model at different locations of one wave length in Maxsurf stability (Version 20).

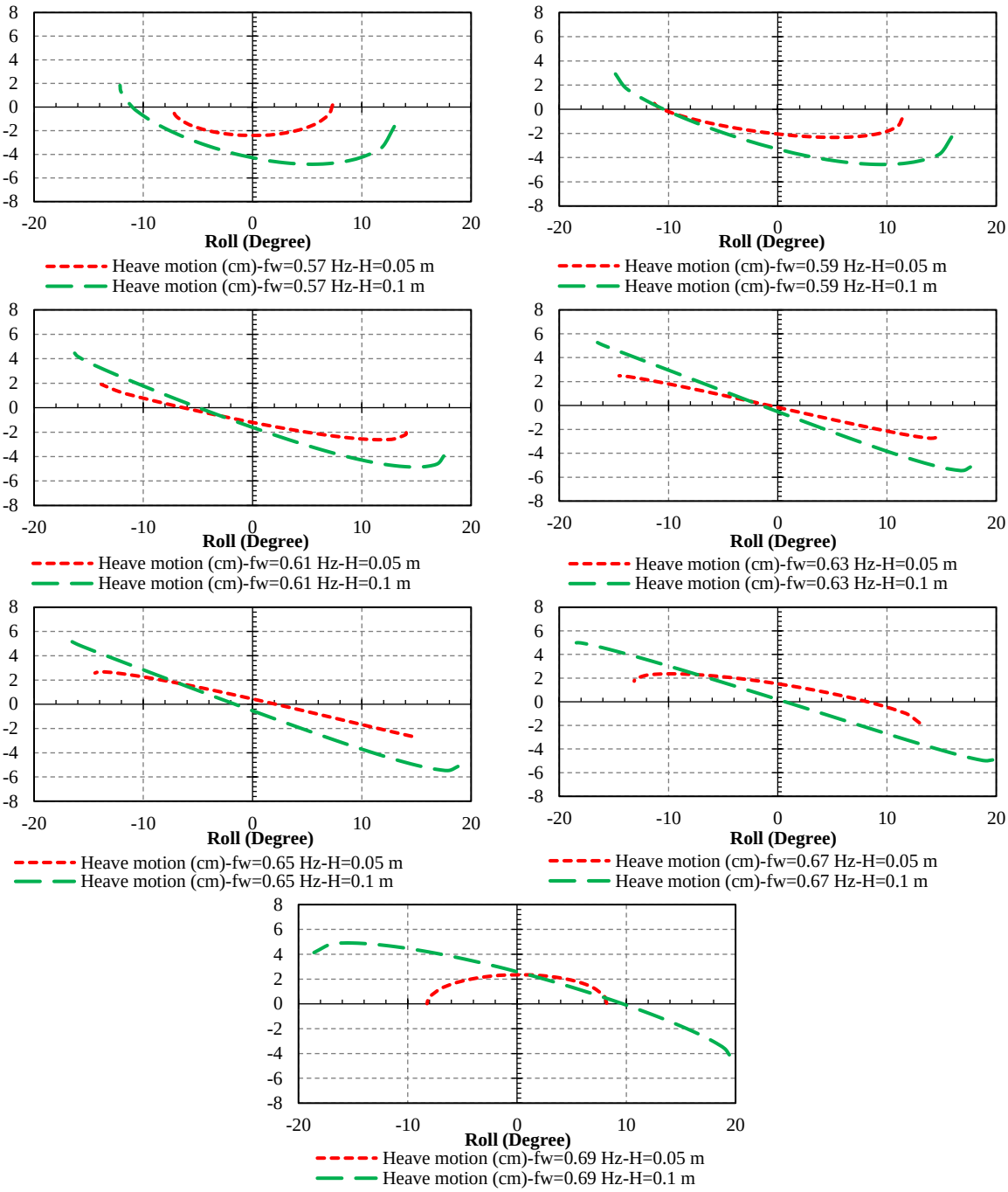

Figure 6.9 The heave motions of the model for different roll angles at wave heights of 0.05 and 0.1 m and wave frequencies (f_w) from 0.57 to 0.69 Hz.

responses of the model at different conditions are quite nonlinear compared to the static condition. When the wave height is small (H=0.05 m), the model has almost the same roll motion characteristics while remaining both in the crest and trough conditions. However, for a larger wave height (H=0.1 m), where the wave has a

sharp crest and a wide trough (trochoidal wave), the roll amplitude at higher wave frequencies is larger in the trough than in the crest condition (up to 2 degrees). On the other hand, the roll acceleration amplitude in the crest condition is larger than the trough condition, since the changes in roll velocity are larger because of experiencing the sharp wave crest. The heave motion of the model remains the same for both crest and trough conditions at a wave height of 0.05 m. Increasing the wave frequency at a larger wave height increases the heave motion due to an increase in the wave steepness.

6.7.2 Restoring moment calculation

It was found that magnitude of restoring moment in waves considering dynamic condition is different from the calm water condition. It depends on the heave motion of the model and location of the crest and trough of a wave with respect to the model. The buoyancy force is a product of total pressure and the wetted surface area in the Z direction. Figure 6.9 illustrates the heave motion of the model at different wave frequencies and wave heights. The model has maximum and minimum roll angles at the trough and crest, when the wave frequency is close to the natural frequency of the model. For the wave heights of 0.05 and 0.1m, the wave frequencies of 0.65 and 0.67 Hz appear closer to the natural frequency. It is shown that when the model is located over the crest, the buoyancy force is smaller than the calm water condition, but it is larger when the model is located in the trough of a wave. When the model experiences a maximum roll angle either in the trough or crest, the variation of buoyancy and roll restoring moment is significantly bigger. It can be seen in Figure 6.10 that the variation of buoyancy for the larger wave height is significant, especially for the case of H=0.1 m and a wave frequency of 0.67 Hz (up to 110 N).

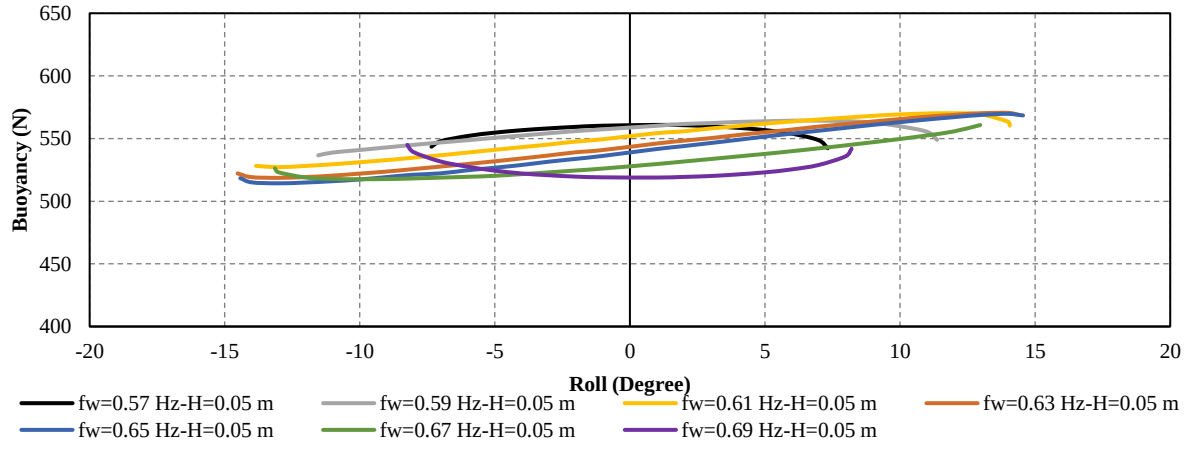

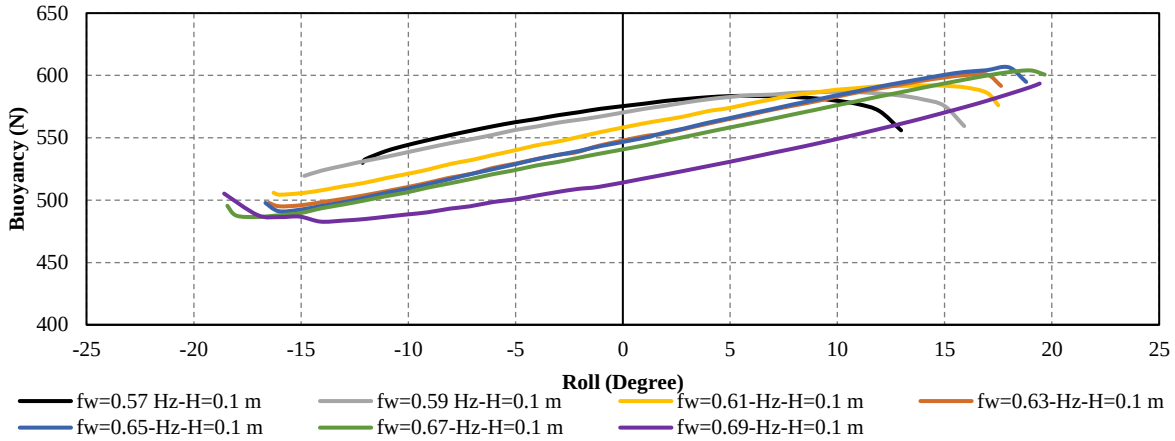

Figure 6.10 Buoyancy variations of the model for different roll angles at wave heights of 0.05 and 0.1 m and wave frequencies (f_w) from 0.57 to 0.69 Hz.

In this study, the centre of floatation (C_F) and the centre of buoyancy (C_B) were calculated at each time step. The centre of floatation is the centre of instant waterplane area, while the centre of buoyancy is the centroid of the underwater volume. The magnitude of restoring moment (M_{Res}) is calculated by equation 6.22, where, M_{C_F} is the total moment around the centre of floatation, d_1 and d_2 are the distances between the centre of floatation and the centres of buoyancy and gravity (C_G), respectively (see Figure 6.11). F_B and W are buoyancy force and weight of the model.

$$M_{C_F} = M_{\mathrm{Res}} = F_B \times d_1 + W \times d_2 \tag{6.22}$$

The investigation of the dynamic responses of the model in waves was shown that the position of waves with respect to the model is one of the main reasons for the restoring moment variation. Figure 6.13 shows the position of free surface at both sides of the model for three different wave frequencies of 0.57, 0.63 and 0.69 Hz. These figures were captured while the model was in the regions 2 and 3 marked in Figure 6.12. The red lines in Figure 6.13 show the free surface in calm water. The restoring moment for the different roll angles is calculated for the calm water by CFD simulations, and the results were equal to the results obtained from Maxsurf. At the wave frequency of 0.57 Hz with the larger roll angle (12.5 degrees), a part of buoyancy from the low side moves to the opposite side because of the wave profile. Therefore, the location of centre of buoyancy comes closer to the centre of gravity compared to the calm water condition. Hence, the magnitude of roll restoring moment is relatively smaller than the calm water condition for the same roll angle (Figure 6.14). In contrast, for the higher wave frequency (0.65 Hz), the buoyancy in the low side is greater; hence, the restoring moment is larger than the calm water condition. It can be seen in Figure 6.14 that the restoring moment is not zero at the zero roll angle due to the effect of the wave position (Figure 6.13). The magnitude of restoring moment recorded for region 3 is smaller than region 2 and the calm water condition. That is because, the buoyancy force is smaller and the distance between the centres of buoyancy and gravity is also smaller, as a result of wave position. The most prominent finding from the plots of Figure 6.13 is that magnitude of restoring moment for the same roll angle at two different wave heights of 0.05 and 0.1 m is different due to differences

in heave motion of the model and wave position. In light of above, the magnitude of roll restoring moment depends on the wave height and wave frequency, and can be larger and smaller than hydrostatic roll restoring moment. Hence, taking into account the hydrostatic restoring moment values in dynamic stability investigations increases the errors of the simulations.

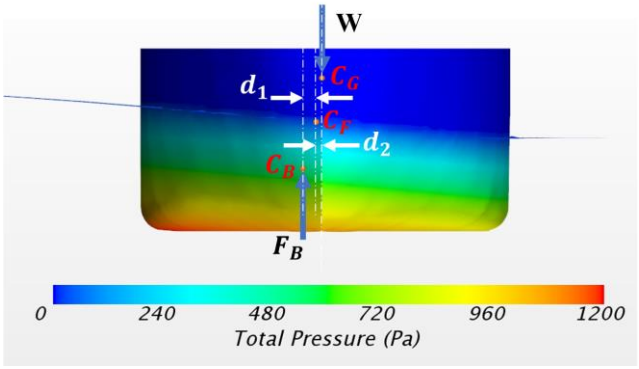

Figure 6.11 Free body diagram for the roll restoring moment calculation

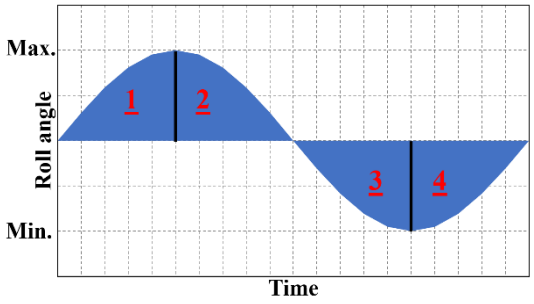

Figure 6.12 Zones for the roll angle variation versus time

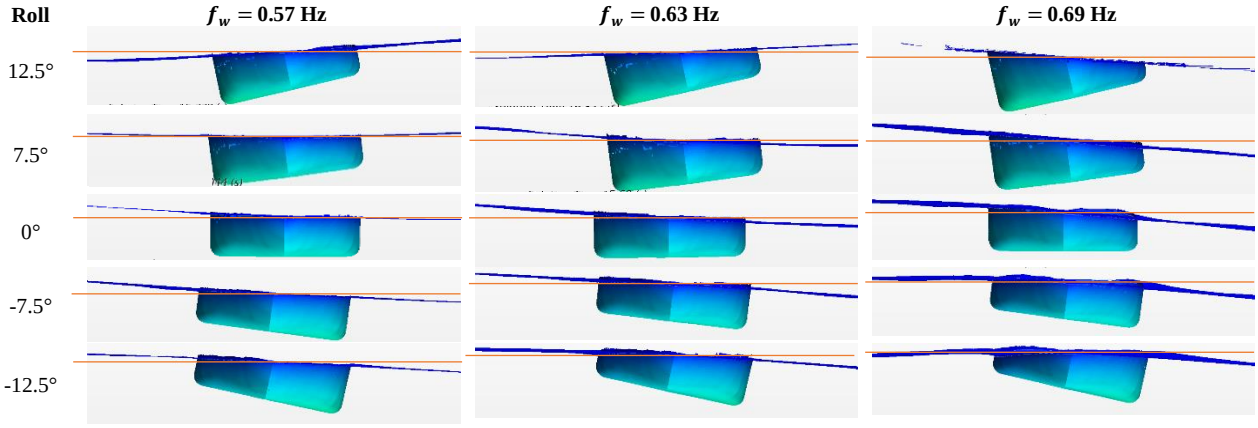

Figure 6.13 Location of the waves with respect to the model at different roll angles and wave frequencies (f_w) for the wave height of 0.1m.

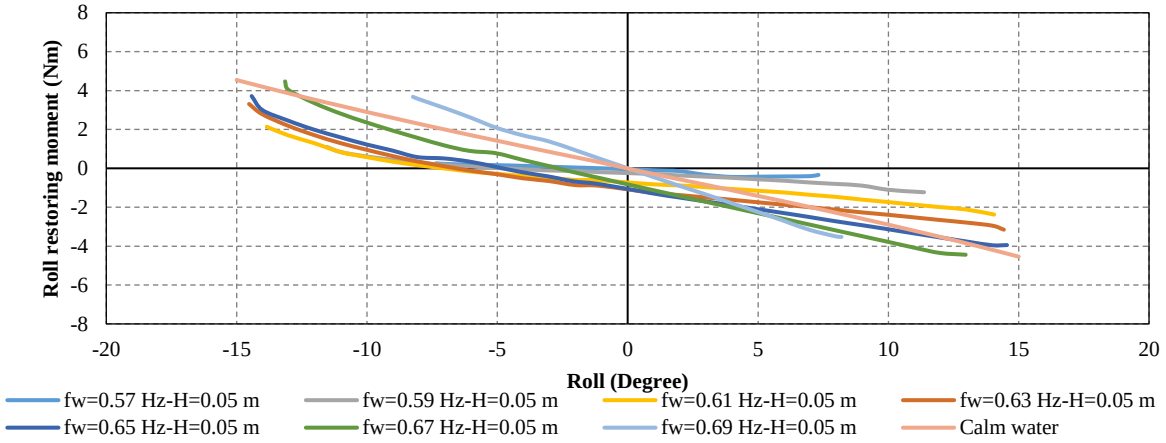

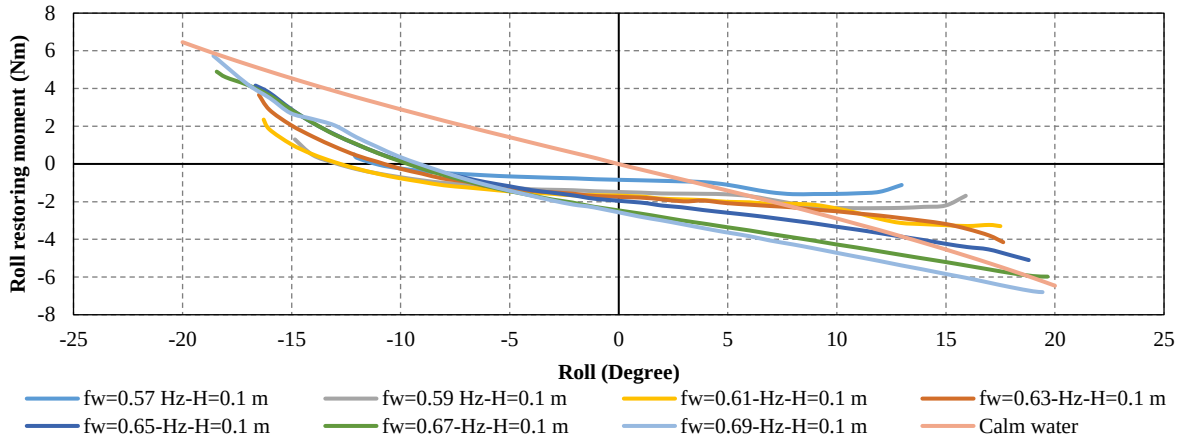

Figure 6.14 Roll restoring moment variations for different roll angles at wave heights of 0.05 and 0.1 m and wave frequencies (f_w) from 0.57 to 0.69 Hz.

6.8 Concluding remarks

Numerical and experimental simulations were carried out in beam sea conditions to study the motion characteristics and roll restoring moment variation at different waves heights and wave frequencies. It was observed that the model has larger motion characteristics close to the natural frequency of the model. At the small wave height (H=0.05), the motion characteristics measured for the wave crest and trough conditions showed the same behaviour as the wave has an identical crest and trough profiles. However, for the wave height of 0.1 m, the wave produces sharper crest and wider trough; hence, the roll amplitude measured in trough condition appeared larger. While, the amplitude of angular acceleration in a wave crest is greater due to larger angular velocity changes.

It was found that the magnitude of restoring moment depends on the magnitude of buoyancy force and the location of the wave crest and trough. Therefore, the magnitude of restoring moment in a dynamic condition can be smaller or larger than the static condition. When the model is located in trough of a wave, the magnitude of buoyancy and the distance between the centre of gravity and centre of buoyancy are larger; thus, the magnitude of restoring moment appears larger than the condition where the model is in the crest.

These findings contribute in several ways to our understanding of ship stability and provide a basis for considering dynamic behaviour in the operational limitations. Further research could usefully explore the sensitivity of different hull forms to variation of the resorting moment in waves.

Chapter 7: Roll added mass moment of inertia and damping calculations in regular beam waves

This chapter has been submitted for publication in journal of Ocean Engineering, and at the time of writing the thesis was under review. The citation for the research article is:

KIANEJAD, S., ENSHAEI, H., DUFFY, J. (2019). Calculation of roll hydrodynamic coefficients in regular beam waves. Ocean Engineering (under review).

Abstract

Simulation of a ship's roll motion through equation-based approaches requires restoring moment, added mass moment of inertia and roll damping coefficients to be known. Accurate estimation of these coefficients will enhance the prediction of ship roll response at a resonance condition. However, the magnitude of these coefficients in regular beam seas and close to a resonance condition is unknown. The present study adopts numerical and experimental simulations to investigate the effects of different wave heights and wave frequencies on ship motion characteristics. The motion characteristics results from numerical simulations are compared against experimental measurements and a good correlation is achieved. The restoring moment in dynamic conditions is calculated and compared to the hydrostatic restoring moment. The dynamic restoring moment is greater than hydrostatic restoring moment for some wave frequencies and smaller for other wave frequencies. The magnitude of roll damping and added mass moment of inertia coefficients is calculated at different wave heights and frequencies and the results yield that there is quite a nonlinear relationship between the roll hydrodynamic coefficients and roll motion characteristics.

Keywords: *Motion characteristics, Added mass moment of inertia Damping coefficient, Restoring moment, Resonance, CFD.*

7.1 Introduction

Reducing the motions of a ship in a seaway is considered paramount in the ship design process. Roll motion is highly nonlinear and limiting its development reinforce the safety level and habitability. Calculating the nonlinear roll damping and added mass moment of inertia coefficients in real sea conditions are significant factors in the accurate prediction of roll motion. In the past, the most common approaches for estimating these coefficients are empirical formulas, model tests or using secondary data from the model tests. Potential theory-based methods have also been used to assess ship motions. They can simulate a ship's motions with reasonable accuracy, except for the roll motion. Because of overlooking the viscosity effects particularly at frequencies close to the roll natural frequency of a ship, where the ship might experience large roll motion. Since the magnitude of those coefficients are related to the viscous flow effects around the body, the experimental or numerical methods should be used to consider these effects. Due to this, recently the focus has changed towards experimental and numerical simulations, especially the use of CFD methods. The literature review consists of two sections including previous works on the calculation of roll damping and added mass moment of inertia.

7.1.1 Damping calculation

Na et al. (2002) carried out experimental simulations based on a harmonic force roll motion technique on a rectangular box with and without bilge keels. The bilge keel geometry was changed in terms of width and the attached angle to investigate the influences on the damping coefficient. Jung et al. (2005), used particle imaging velocimetry (PIV) to track the vortex and turbulence generation in roll motion of a box in beam waves. The rate of generated vortex and turbulence were higher on the seaward side of the box and the vorticity and turbulence

intensity were related to the wave transmission. Fixing the box increases the turbulence intensity because the relative velocity around the box arises. It was observed that flow near the corner of the box is more turbulent due to separation. Yi-Hsiang et al. (2005) conducted a 2D CFD study to simulate the harmonic force roll motion of a FPSO section, with and without bilge keels. It was reported that added bilge keels at 45 degrees inclination increased the added mass moment of inertia and damping. While the amplitude of added mass moment of inertia remained unchanged with both horizontal and vertical bilge keels, the damping amplitude was larger with horizontal bilge keels. Yu and Kinnas (2009) employed a 2D incompressible Navier-Stokes solver to study the roll damping of a rounded bilge box with and without bilge keels, and additionally a sharp corner bilge box with and without a step at the bilge keels. The exciting moment was applied to the model free in roll motion. It was observed that adding bilge keel increased the amplitude of damping and the relation between the variation of roll moment and roll angle was nonlinear due to viscosity effects. To study the roll damping of a rectangular barge, Bangun et al. (2010) conducted a numerical simulation using 2D incompressible Navier-Stokes solver. The model was considered with and without bilge keels, where the width and angle of bilge keel were changed for 12 sets of tests. They concluded that the barge with a smaller bilge keel angle from the horizontal axis experienced larger roll damping. Thiagarajan and Braddock (2010) accomplished experimental and numerical studies of a FPSO model in a forced roll motion technique using 1:350 scaled ship model. The numerical simulations based on Free Surface Random Vortex Method (FSRVM) were in a good correlation with the experimental results. They concluded that the amplitude of damping is a function of roll angular velocity and the width of bilge keel. An equation was proposed based on the relation between damping ratio, width of the bilge keel and barge beam, considering few assumptions. Irkal et al. (2016) investigated the impact of different bilge keels on the roll damping using numerical and experimental simulations. They used PIV method for the experiments to measure the velocity field around the model during the free oscillation tests. They pointed out that the roll damping coefficient of the model in the bare hull condition is linear, whereas, the roll damping of the fully appended condition is strongly nonlinear.

Avalos et al. (2014) performed a numerical simulation to study the roll decay of a FPSO with and without bilge keels, and the results were in agreement with the experiment. It was noticed that the size of the vortex is a function of the roll motion amplitude and width of the bilge keel. Wilson et al. (2006) used CFD method to simulate roll decay of a surface combatant with and without bilge keels in different Froude numbers. The calculated roll damping coefficients for low Froude number were in good agreement with experimental measurements, while the results of high Froude number had 20 % deviation. Yang et al. (2013) performed numerical simulations to compute the roll damping for both roll decay and forced rolling of DTMB 5512 and S60 hulls in different Froude numbers. They found that the roll amplitude and forward speed have more influence on roll damping compared to the frequency of excitation. Gao and Vassalos (2011) conducted numerical simulations for roll decay of DTMB 5415 in intact and damage condition. The model was equipped with bilge keels and the calculated roll damping was smaller than the model tests results. Begovic et al. (2015) carried out CFD simulations using STAR CCM+ to calculate the roll damping of DTMB 5415, using roll decay technique for both intact and damage conditions. The results were compared against experimental measurement

and found a reasonable accuracy. Mancini et al. (2018) carried out roll decay tests using numerical and experimental simulations to calculate the roll damping coefficients. For the numerical uncertainty analysis, the grid convergence index was used instead of the correlation factor method, because the solutions were not close to the asymptotic range. Zhou et al. (2015) performed numerical and model test measurements to compute the roll damping of four different ship models by using roll decay technique at Froude number of zero. The simulation results had a good correlation with the experimental measurements.

To estimate the roll damping coefficient of a ship, the roll decay technique is not a suitable method for large roll motions, especially in forward speed. Harmonic excited roll motion (HERM) technique proposed by Blume (1979) can precisely calculate roll damping coefficient in the aforementioned conditions. This method is based on exciting the model at the resonance frequency. The main drawback of this technique is the long simulation time to measure the resonance frequency. Another disadvantage is the dependency of roll damping coefficient on maximum roll angle, metacentric height and heel angle. Each of these items should be recorded and could be subject to errors, as a result, the uncertainty of Blume's method is high. Handschel and Abdel-Maksoud (2014) presented an improved HERM technique to estimate the damping coefficient for a range of frequencies very close to the resonance frequency. They measured the phase shift between the exciting moments and the roll angles for other than 90 degrees. The advantages of their method are twofold; the measuring time is reduced to the range of roll decay method, and no further modification for the test set up is required. Wassermann et al. (2016) conducted several model tests based on the roll decay and HERM technique to calculate the roll damping of a post panamax container ship model. They introduced different approaches for roll damping calculation without additional filtering, curve fitting, and offset manipulation for the recorded time series. Oliva-Remola et al. (2018) carried out the HERM technique by shifting a mass harmonically inside the model in the y-direction to excite the model, where masses were used to generate different roll angles. For the same roll angle, the calculated roll damping was smaller from HERM technique than the roll damping from roll decay tests. That is because, the roll damping is calculated when the roll angle reaches a steady condition in HERM technique, whereas the roll damping in the roll decay is calculated when the model is in a transient condition.

Somayajula and Falzarano (2017a) introduced an advanced system of identification to estimate frequency dependent roll damping from results of experimental measurements in irregular waves. The proposed method predicted the roll motion of the model precisely in comparison to the potential flow and empirical methods.

7.1.2 Added mass moment of inertia calculation

Salvesen et al. (1970) utilised the strip theory method to calculate 2D sectional added mass in roll motion and then 2D sectional added mass was integrated over the length of the ship to compute the 3D added mass moment of inertia. To integrate the 2D sectional added mass over the length, Das et al. (2006) used applied Frank Close-Fit method. The magnitude of the roll added mass moment of inertia varies between 10-25 percent of the roll mass moment of inertia for displacement ships based on the potential flow approaches (Bikdash et al., 1994, Grinnaert et al., 2016, Schumacher et al., 2016, Taylan, 2003, Wright and Marshfield, 1979).

Due to the limitations of strip theory in accounting the impact of viscosity and turbulent flow around a ship, especially in the roll motion, Subramanian (2012) applied an empirical correction to include the viscous effect. Jaouen et al. (2011) carried out CFD simulations on a ship hull section to consider the viscous effects. They submerged the model to remove the restoring moment, and calculated the roll added mass moment of inertia using Fourier series. Discusser et al. (2014) used Reynolds-averaged Navier-Stokes (RANS) method to capture the flow behaviours around the model for calculating the added mass. Judge (2010) conducted a series of model tests at different forced roll angles, forward speeds, and excitation frequencies. They observed that for a high range of frequencies, the variation of frequency has a negligible impact on the magnitude of roll added mass moment of inertia, while, the magnitude at a low range of frequencies depends on the frequency as well as forward speed. Judge and Judge (2013) calculated the roll added mass moment of inertia of a planning hull based on the forced roll oscillation and investigated the impact of the forward speed and roll amplitude. They observed that the magnitude of roll added mass moment of inertia is independent of the roll amplitude, whereas, increasing the forward speed reduces its magnitude. Bhattacharyya (Bhattacharyya, 1978) performed analytical and experimental simulations to estimate the roll added mass moment of inertia. He concluded that the roll added mass moment of inertia of a ship is about 20% of the roll mass moment of inertia. Kianejad et al. (2019b) and Kianejad et al. (2017) proposed a method based on the HERM technique to compute the roll added mass moment of inertia of a post panamax container ship using CFD simulations. They found that the magnitude of roll added mass moment of inertia coefficients of a bare hull model is smaller than the fully appended model, and the full-scale ship has a smaller added mass moment of inertia due to a smaller phase shift and angular acceleration. They also noticed that the magnitude of roll added mass moment of inertia depends on forward speed, roll angle, and excitation frequency.

In light of the above, the roll damping and added mass moment of inertia are significant to precisely predict a ship motions at a range of frequencies close to the resonance frequency of a ship. While, the magnitude of these coefficients is unknown in waves conditions. In this study, CFD simulations and experimental measurements were performed in 35 cases in regular beam sea conditions to investigate the influence of five wave heights (0.025, 0.05, 0.075, 0.1 and 0.125 m) and seven wave frequencies which were close to the natural frequency of the model (from 0.57 to 0.69 Hz with intervals of .02 Hz) on roll motion characteristics. After validation of the CFD method against experimental model tests, the CFD simulations were used to compute the roll exciting and restoring moments as the calculation of their magnitudes were not feasible in experimental measurements. In the next step, the roll added mass moment of inertia and roll damping coefficients were calculated in different conditions.

7.2 Model geometry

Please refer to section 6.2.

7.3 Experimental measurements

Please refer to section 6.3.

7.4 Numerical modelling

Please refer to section 6.3.

7.4.1 Governing equations and physics modelling

Please refer to section 6.4.1.

7.4.2 Mesh structure and generation

Please refer to section 6.4.2.

7.4.3 Boundary and initial conditions

Please refer to section 6.4.3.

7.5 Experimental uncertainty

Please refer to section 6.5.

7.6 Numerical uncertainty analysis

Please refer to section 6.6.

7.7 Results and discussion

The motion amplitudes predicted using CFD are compared to the experimental measurements for various wave heights and wave frequencies. The exciting moment and restoring moments are calculated and the latter is compared against the restoring moment corresponding to the hydrostatic condition. The non-dimensional roll damping and added mass moment of inertia are calculated when the model is located in crest and trough of a wave. In the following sections, the model is located in the crest and trough conditions reflect that the model is located in zones 1 and 2, respectively (Figure 7.1).

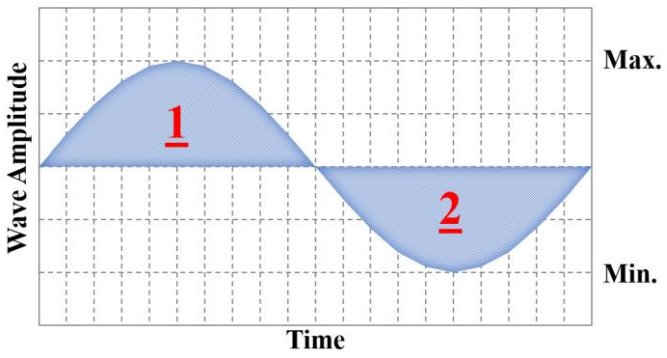

Figure 7.1 Zones for the crest (1) and trough (2) conditions.

7.7.1 Motion characteristics

The motion characteristics of the ship model including roll angle, roll angular velocity, roll angular acceleration and heave motion for different wave heights and wave frequencies are shown in Figure 7.2. In

general, there is a good correlation between numerical and experimental results. For each one of the motion characteristics, two figures are presented where the left-hand figures are recorded when the model was in the trough of a wave and the right side for the crest condition. It is apparent that increasing the wave height increases the roll angle, however, the responses of the model to the different wave heights and wave frequencies are nonlinear. For the smaller wave heights of 0.025 and 0.050 m, increasing the wave frequency increases the roll angle to reach the maximum value at a wave frequency of 0.65 Hz which is very close to the natural frequency of the model, however, reduction in the roll angle is apparent beyond this wave frequency. At the larger wave heights of 0.1 and 0.125 m, increasing the wave frequency increases the roll angle and the maximum roll angle occurs at a frequency of 0.67 Hz and further increase of the wave frequency slightly decreases the roll angle. This is because the natural frequency of the model varies depends on the roll angle, and for the larger wave heights or roll angles, it shifts towards the larger magnitude (Kianejad et al., 2019b, H. Enshaei, 2018). The roll angular velocity and acceleration have the same trends as the roll angle. The maximum values occur at the resonance condition and their magnitudes decline at wave frequencies away from the resonance. The magnitude of roll angular velocity and acceleration is larger at a higher frequency for the same roll angle (at wave height 0.025 and 0.050 m) due to larger excitation frequency. It was observed that the magnitudes of roll angles for the crest and trough conditions are the same at smaller wave heights, because the wave profile is the same for the crest and trough conditions (Figure 7.3). While for the larger wave heights, the wave crest is sharper and the wave trough is wider, there are roll angle differences between the trough and crest conditions, especially at higher wave frequencies. On the other hand, the magnitude of roll angular acceleration of the model at the crest condition is larger as the roll velocity changes are larger because of the sharper wave crest. The heave motion amplitude for the crest and trough conditions are almost the same. For the smaller wave heights, the model experiences slightly larger heave motion at a wave frequency of 0.65 Hz compared to the other wave frequencies. While, at larger wave heights, increasing the wave frequency increases the heave motion magnitude as the wave steepness increases.

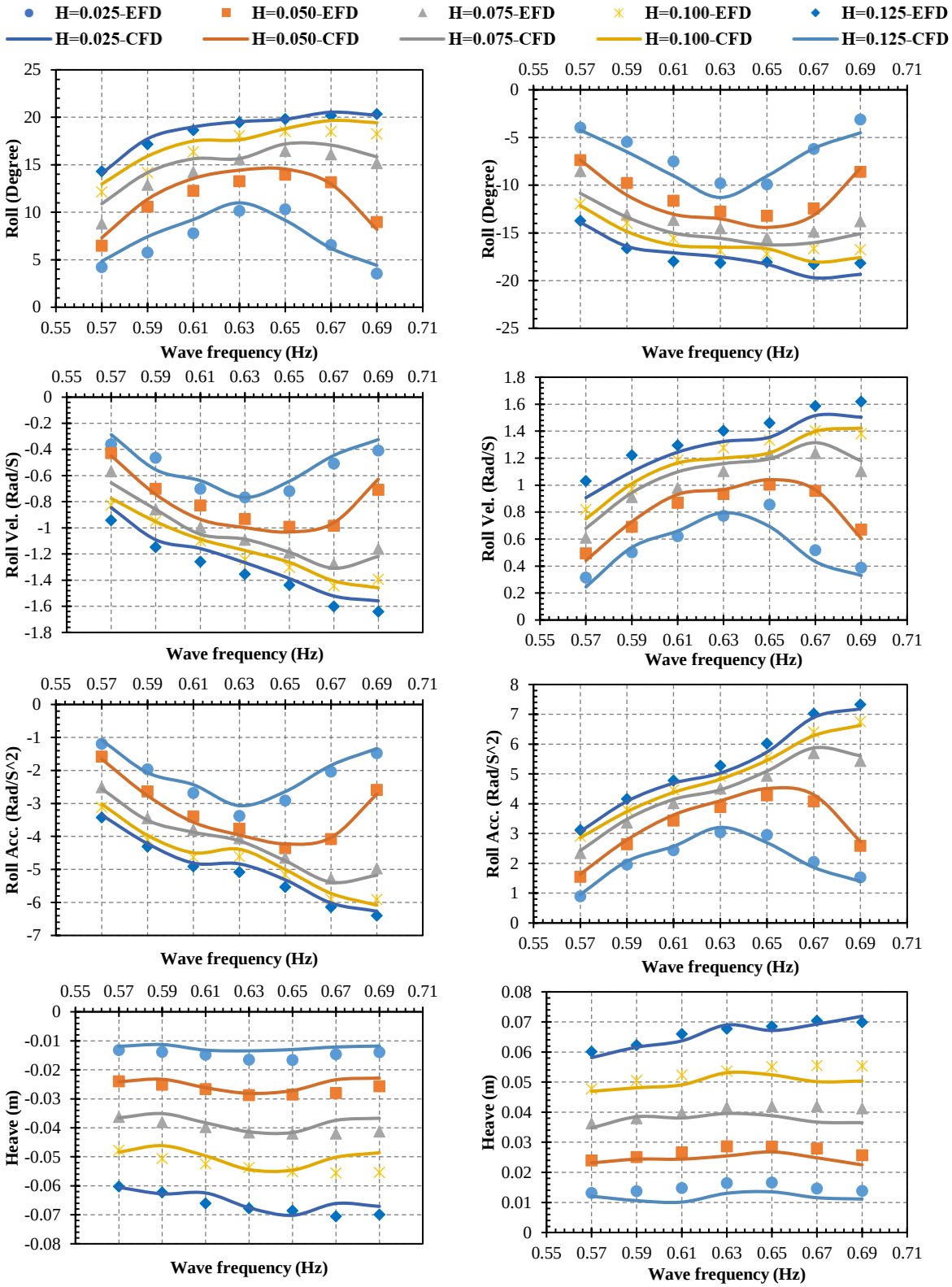

Figure 7.2 Amplitude of roll angle, roll angular velocity, roll angular acceleration and heave motion of the experimental and numerical simulations at different wave heights (H=0.025 to 0.125 m) and frequencies (0.57 to 0.69 Hz) both for the trough (figures in the left side) and crest (figures in the right side) conditions. EFD denotes results from experimental measurements.

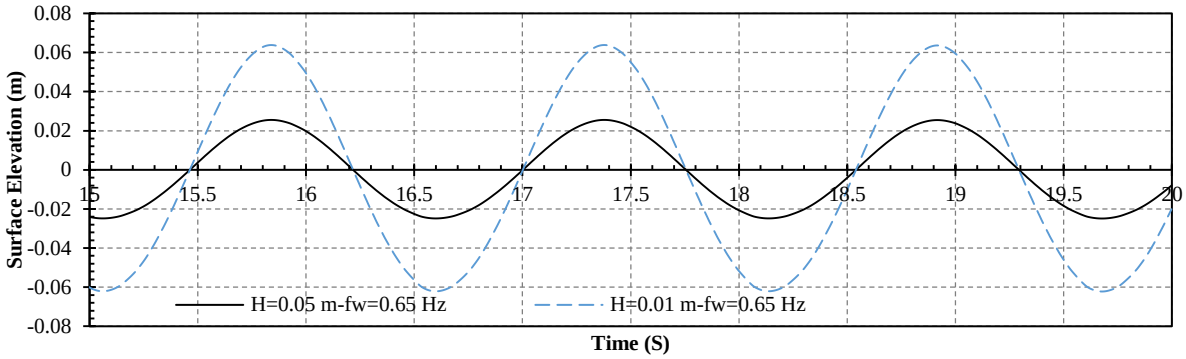

Figure 7.3 Surface elevation time traces at two wave heights of 0.050 m and 0.125 m and a wave frequency of 0.65 Hz.

7.7.2 Roll restoring moment calculation

Please refer to section 6.7.2.

7.7.3 Roll exciting moment calculation

The exciting moments induced on the model from the waves are calculated by the following equation as can be seen in Figure 7.5, where, F_L and d are the lateral force from the wave and its lever to the centre of floatation.

$$M_{C_{F_2}} = M_{Exc.} = F_L \times d \tag{7.1}$$

The magnitude of the exciting moments for various roll angles at different wave frequencies and a wave height of 0.1 m are shown in Figure 7.4. As the half cycle of a wave (trough to crest) was selected to investigate the roll exciting and restoring moments, the magnitude of exciting moment is positive and in the next cycle (crest to trough) is negative. The exciting moment has maximum value when the model has zero heave motion, because the slope of the free surface at the zero wave elevation is maximum. For the positive roll angles, the exciting moment contributes to increase the roll angle while for the negative roll angles it opposes the roll angle development. Increasing the wave height increases the variation and magnitude of exciting and restoring moments. As mentioned above, the magnitude of roll restoring moment varies at different wave heights and frequencies even for the same roll angle, thus, considering the restoring moment from hydrostatic calculation is far from reality and increases the discrepancies of the simulations.

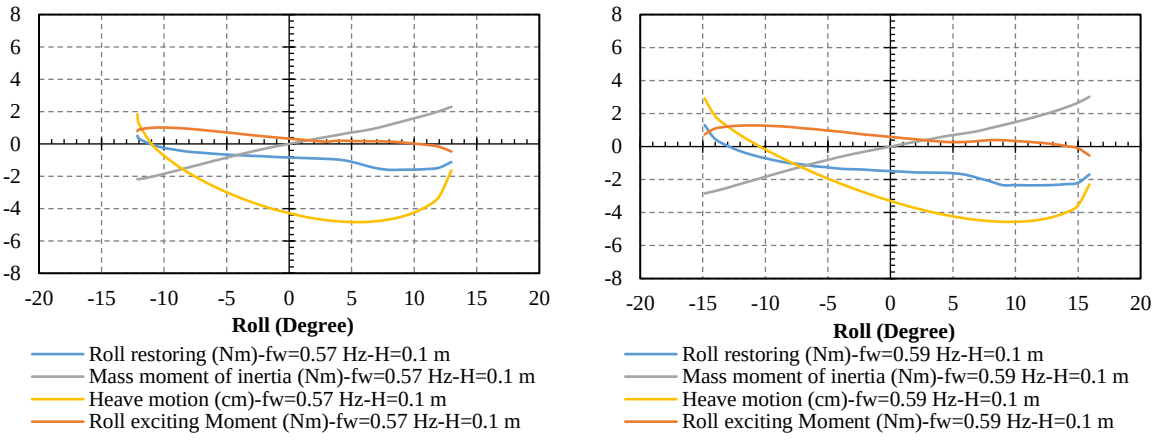

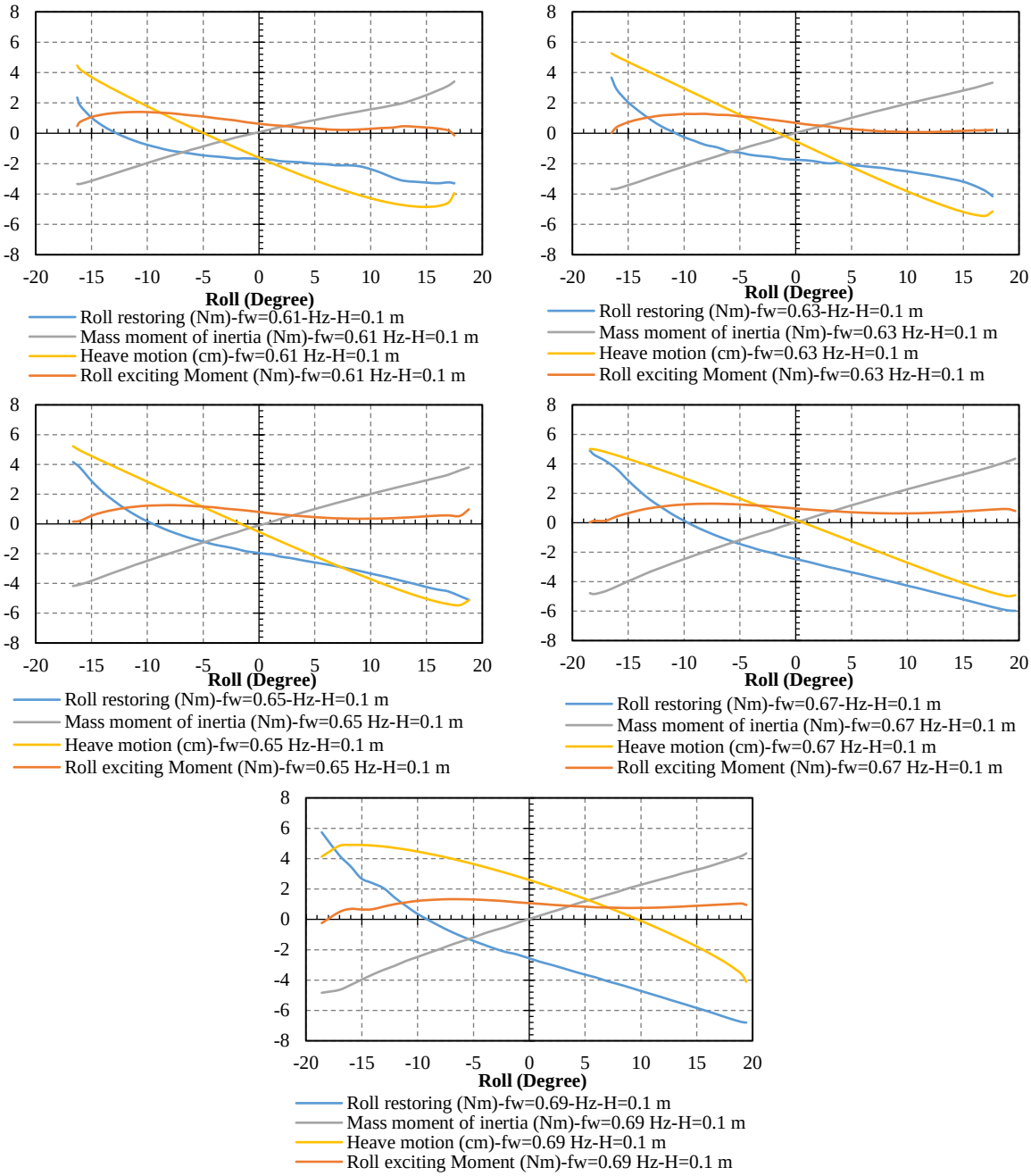

Figure 7.4 Heave motion, roll restoring, mass moment of inertia and roll exciting moments variations for various roll angles at a wave height of 0.1 m and different wave frequencies (f_w).

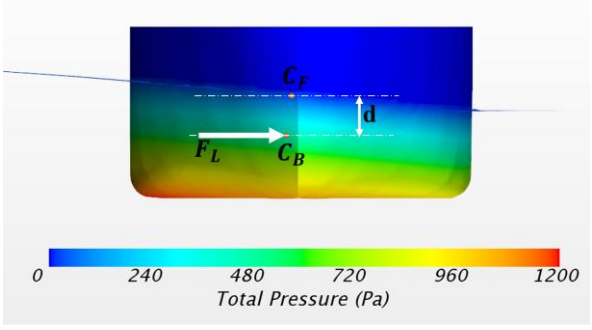

Figure 7.5 Free body diagram for calculation of the roll exciting moment.

7.7.4 Roll added mass moment of inertia coefficient

The equation of rotational motions including roll in a body local system regarding the centre of gravity is (Kianejad et al., 2019a):

$$I\frac{d\omega}{dt}+\omega\times I\omega=M=M_p+M_v \tag{7.2}$$

Where, I and ω represent the tensor of mass moment of inertia and angular velocity of the model, M is the moment on the model and indices of p and v are the pressure and viscous parts. By restraining the model in sway and yaw motion, the magnitude of these motions was decreased, however, the model remains free in 6 DOF and different motions influence on other motions. The focus of this study is calculation of the roll motion coefficients, hence, the 6 DOF equations of motion can be simplified into a 1 DOF equation as below where the hydrodynamic coefficients are still under the influence of the all motions.

$$(I_{44}+\delta I_{44})\ddot{\varphi}_4+N_{44}\dot{\varphi}_4+S_{44}\varphi_4=M_{Exc.44} \tag{7.3}$$

In the equation above, I_{44} and δI_{44} are the roll mass and added mass moment of inertia coefficients. N_{44} and S_{44} represent the roll damping and restoring coefficients, respectively. It is known that there are linear and nonlinear relations between the hydrodynamic coefficients and roll motion characteristics as discussed in the next sections. The model reaches the steady-state condition after a couple of cycles and maintains the same amplitude of roll motion characteristics in the following cycles. The computation of roll motion coefficients was conducted for a couple of cycles which had the same amplitude of roll motion characteristics. When the model has maximum or minimum roll angle in the trough and crest of a wave, the angular velocity of the model is almost zero (the damping moment is negligible), and the roll added mass moment of inertia can be computed by equation 7.3 (Kianejad et al., 2019b) as the other moments including the exciting moment, restoring moment and roll mass moment of inertia are known over the simulation's time (Figure 7.4). The magnitude of roll added mass moment of inertia coefficients at different wave heights and frequencies both for the trough (left hand) and crest (right hand) conditions are shown in Figure 7.6. It is made non-dimensional dividing by the roll mass moment of inertia. The magnitude of roll added mass moment of inertia coefficients for different wave heights at lower wave frequencies has smaller difference as the conditions are far from the resonance condition, while the differences increase at higher wave frequencies as the model at the larger wave heights experiences the resonance at higher frequencies. The coefficients at smaller wave heights and higher wave frequencies are larger because of the smaller induced acceleration, while, the magnitude of roll added mass moment of inertia moments at the larger wave heights are greater. The magnitude of roll added mass moment of inertia coefficients at lower wave frequencies are negative which implies that they act against the roll motion development. It is mainly because of the location of the model with respect to (Figure 7.4), where it has smaller heave motion and is far from the crest and trough. Hence, the rate of change of flow velocity (acceleration of the flow around the model) is larger than acceleration induced by the model and in the opposite direction of the model rolling direction as can be seen in Figure 7.7. At higher wave frequencies, the model experiences the maximum /minimum roll

angle at the trough and crest conditions where the flow acceleration induced by the model is dominant as the flow velocity variation is small. The roll added mass moment of inertia coefficient at low wave frequencies for the model in trough and crest conditions have the same values. Whereas, for the larger wave heights and higher wave frequencies, the crest conditions have smaller values because of the larger acceleration (larger moment of roll mass moment of inertia).

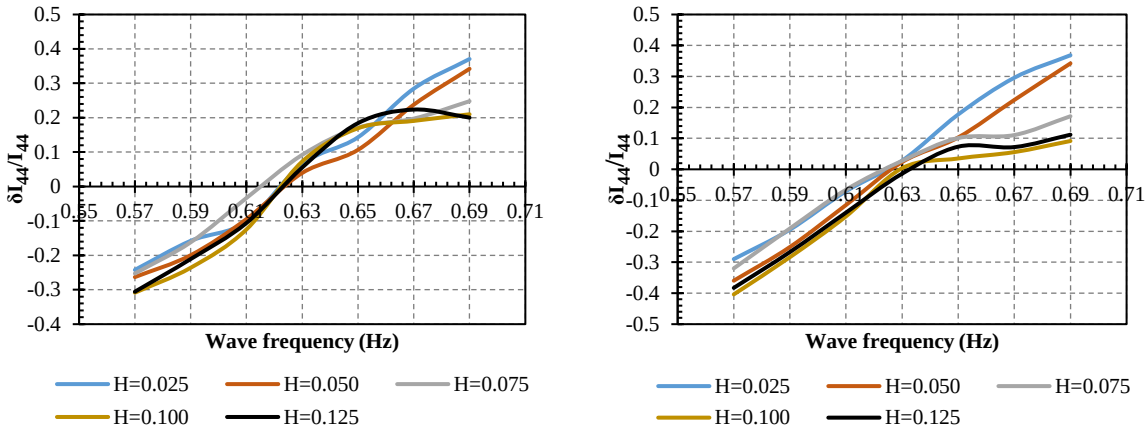

Figure 7.6 The non-dimensional roll added mass moment of inertia coefficient of the model at different wave heights (H) and wave frequencies both for the trough (figures in the left side) and crest (figures in the right side) conditions.

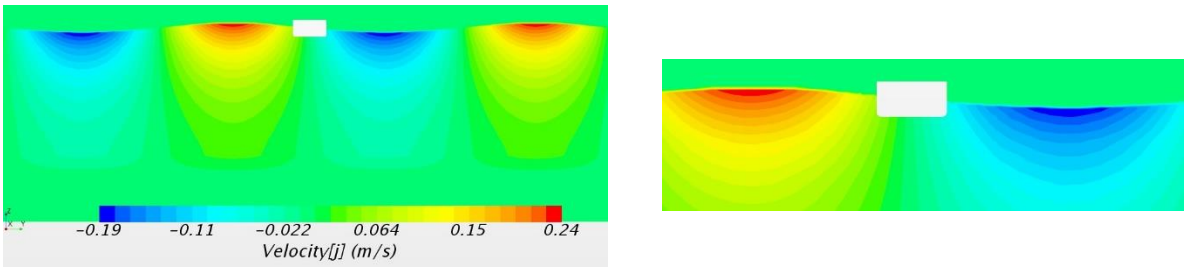

Figure 7.7 Flow velocity contour around the model (at midsection) at a wave frequency of 0.65 Hz and a wave height of 0.1 m.

7.7.5 Roll damping coefficient

The roll damping is calculated using equation 7.4 when the roll angle is small (the roll damping moment is maximum), and the corresponding restoring, exciting and virtual mass moment of inertia moments were calculated as explained in the previous sections. It was assumed in each case that there is a linear relationship between the roll damping coefficient and roll angular velocity, while it has been shown by several researchers that there are both linear and nonlinear relationships between them. Based on the method proposed by Oliva-Remola et al. (2018) and Irkal et al. (2019), and using fitting curve functions the linear and nonlinear parts of the roll damping can be computed from the computed roll damping coefficient considering the linear relationship with the roll angular velocity. Regardless of the roll damping calculation technique, a polynomial expansion of the roll angle or roll angular velocity can be used to approximate the roll damping coefficient (Oliva-Remola et al., 2018) (including linear and nonlinear parts), which is not the focus of this study. The roll damping coefficient can be non-dimensional by equation 7.5 (Reed, 2011). The roll damping coefficients for various wave frequencies at various wave heights for the trough (left hand) and crest (right hand) conditions are shown in Figure 7.8.

$$N_{44} = \frac{M_{Exc.44} - ((I_{44} + \delta I_{44})\ddot{\varphi}_4 + S_{44}\varphi_4)}{\dot{\varphi}_4} \tag{7.4}$$

$$B_{44} = \frac{N_{44}}{\rho \nabla B_{wl}^2} \sqrt{\frac{B_{wl}}{2g}} \tag{7.5}$$

It can be seen that there is a nonlinear correlation between the magnitude of roll damping and the wave height and wave frequency. Increasing the wave height increases the magnitude of roll damping both for the crest and trough conditions, however, the increase is different at different wave heights at each wave frequency. At smaller wave heights, increasing the wave frequency increases the roll damping to reach a peak and after that declines at higher wave frequencies. Since the condition moves away from resonance condition and roll motion decreases. In contrast, at larger wave heights where the higher wave frequencies are closer to the natural frequency of the model, increasing the wave frequency increase the magnitude of roll damping coefficients. The magnitude of roll damping at lower wave frequencies for both the trough and crest are almost the same, while at higher frequencies, the crest condition has large values due to greater excitation force due to the larger free surface slope. As above, the magnitude of hydrodynamic coefficients in regular beam sea conditions are different compared to the still water condition and this should be taken into account to improve ship roll motion prediction.

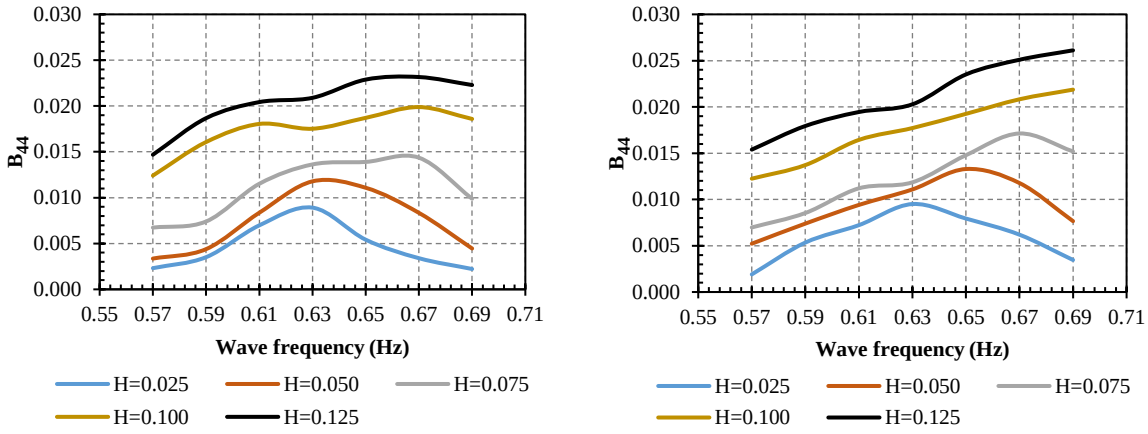

Figure 7.8 The non-dimensional roll damping coefficient of the model at different wave heights (H) and wave frequencies both for the trough (figures in the left side) and crest (figures in the right side) conditions.

7.8 Concluding remarks

Numerical and experimental simulations were conducted in regular beam sea conditions to investigate the influence of wave height and frequency on ship motion characteristics and roll hydrodynamic coefficients. In general, increasing the wave height increases the roll motion while the model experiences the maximum roll motion around the resonance frequency. As at smaller wave heights, the motion characteristics are the same as the surface elevation both in trough and crest are the same. At higher wave heights, the wave has a wider trough and sharper crest, hence, the model remains more time in trough condition, so the induced roll angle is larger. On the other hand, the model has larger roll angular acceleration in crest condition due to larger rate of change of roll velocity.

The magnitude of restoring moment in a dynamic condition can be either smaller or larger than the hydrostatic condition depending on the magnitude of buoyancy force and the position of the wave with respect to the model. The model has larger restoring moment when it is in a trough condition due to the larger buoyancy force and larger distance between the centres of buoyancy and gravity. At lower wave frequencies, the magnitude of restoring moment in dynamic condition is smaller than the hydrostatic condition, however, at higher wave frequencies, the magnitude of restoring moment in dynamic condition is larger. The exciting moment form waves on the model in one-half cycle is positive and turns into negative in the next half cycle, which has its maximum value at a surface elevation of zero due to maximum slope of the free surface.

The magnitude of roll added mass moment of inertia coefficient varies at different wave frequencies. At a low wave frequency, it has negative value which resists the roll motion because of the flow acceleration around the model is dominant and in the opposite direction of the model rolling motion. While, at higher wave frequencies, the coefficients are positive and contribute to the roll motion development. Although, the magnitude of roll added mass moment of inertia coefficients at different wave heights are the same at some frequencies, the magnitude of their moments around the resonance frequency and larger wave height are greater.

It was observed that there is a nonlinear relationship between the magnitude of roll damping and wave height and frequency. The roll damping coefficient around the resonance frequency is larger than other frequencies and the magnitude of roll damping increases by increasing the wave height.

The findings of this study demonstrate the importance of calculating roll added mass moment of inertia, roll damping, roll restoring moment and roll exciting moment using a dynamic approach in order to provide an accurate assessment of a ship roll behaviours.

Chapter 8: Summary and conclusion

8.1 Summary

Numerical and experimental simulations were conducted to compute the roll hydrodynamic coefficients for a post Panamax container ship and a bulk carrier, including added mass moment of inertia, damping, and restoring. In this regard, the influence of several effective parameters like excitation frequency, DOF, Froude number, appendages, and wave characteristics on the magnitude of hydrodynamic coefficients were investigated. It was observed that the CFD methods could be used to precisely compute the roll motion characterises and hydrodynamic coefficients. More importantly, investigating the impact of DOF is just feasible utilising CFD simulations, because, the motions of a model are coupled and have influence on other motions, and it is hard to restrain the model in experimental measurements. In addition, calculating the exciting and restoring moments in waves is possible by CFD, as in experiments the model should be restrained to calculate these moments. The key findings of this study are as follows:

8.2 Key findings in calm water

It was found that at the roll resonance condition, where the phase shift between the roll exciting moment and roll angle is close to 90 degrees, the model absorbs maximum energy from the exciting moment. While, the phase difference between the angular acceleration and roll angles is close to 180 degrees, where the total mass moment of inertia and restoring moment have the same magnitudes but acting in opposite directions to each other. It was fond that for the frequencies less than the resonance frequency, the phase shift between the exciting moment and the roll angle is less than 90 degrees and it reduces further as frequency decreases (Table 2.8). On the other hand, for the frequencies higher than the resonance frequency, the phase shift is greater than 90 degrees, and increases by increasing the excitation frequency. The phase difference between roll angle and angular acceleration for a low range of frequencies is less than 180 degrees, whereas it is larger than 180 degrees for the higher frequencies investigated (Table 2.9).

It was found that variations in the loading condition and weight distribution change the static ship stability significantly, while their effects on dynamic stability (maximum imposed roll angle) are smaller under the same external roll exciting moment. Changing the VCG by 1% changes the restoring moment from hydrostatic calculation and the maximum roll angle in dynamic condition by 20% and 9%, respectively. On the other hand, the variation of the roll moment of inertia by 5% for the same loading condition changes the maximum roll angle by about 7%, while the hydrostatic calculation fails to consider the effects of roll moment of inertia.

It was observed that the non-dimensional roll added mass moment of inertia at model scale is larger than at full scale due to both larger phase shift and angular acceleration (Figure 3.13). A fully appended condition experiences a larger roll added mass moment of inertia coefficient, however, the moment of roll added mass moment of inertia for a bare hull model is larger than a fully appended hull because of both larger induced roll angle and acceleration. Increasing the Froude number and excitation frequency reduces the magnitude of roll added mass moment of inertia coefficient (Figure 3.12). It was also found that the roll added mass moment of inertia varies with the roll angle, and the magnitudes were quantified over a range of roll angles. By increasing

the roll angle, the roll added mass moment of inertia coefficient increases, and approaches a peak value before declining with a further increase of the roll angle.

The phase shift between the roll exciting moment and roll angle for the model-scale and full-scale decreases by increasing the DOF and Froude number (Figure 4.9). Whereas, the fully appended model experiences a larger phase shift than the bare hull model (Figure 4.4 to Figure 4.7). The phase shift at full-scale is smaller than at model-scale due to relatively lower impact from vorticity and viscous effect at the full-scale condition. It was found that adding appendages, decreasing the DOF and increasing the forward speed, decrease the roll motion. However, they increase the damping coefficients for both model-scale and full-scale (Figure 4.11 and Figure 4.12). While comparing the full-scale condition to model-scale, the full-scale generates larger roll motion and smaller non-dimensional damping coefficients in all cases under the same equivalent roll exciting moment. That is because of viscous effects, which is the significant part of the total damping moment and has a lower impact at higher Reynolds number.

The computed restoring moment in dynamic condition was larger than the static condition (Figure 5.8), especially for small roll angles, due to the angular velocity being at the highest value, where dynamic pressure adds up to the hydrostatic pressure. The appendages increase the pressure difference between two sides of the model by generating the vorticity, therefore, the restoring moment of the fully appended condition appears larger than the bare hull condition. Increasing DOF increases the magnitude of restoring moment, and the sway motion specifically has a greater contribution among other motions.

8.3 Key findings in regular beam waves

Increasing the wave height increases the roll motion, and the model experiences the maximum roll motion around the resonance frequency. It is known that at smaller wave heights, the motion characteristics are the same for both in trough and crest conditions (trough and crest mean when the model in located in a trough or crest of a wave as can be seen in Figure 6.6). However, at higher wave heights, the wave has a wider trough and sharper crest, hence, the model remains in the trough condition for a longer period of time, so the induced roll angle is larger. On the other hand, the model has larger roll angular acceleration in the crest condition due to a larger rate of change of roll velocity.

The magnitude of restoring moment in a dynamic condition can be either smaller or larger than the hydrostatic condition (Figure 6.14), depending on the magnitude of buoyancy force and the position of the wave with respect to the ship model. It became evident that the model has a larger restoring moment when it is in a trough condition due to a larger buoyancy force and a larger distance between the centres of buoyancy and gravity. For the lower wave frequencies investigated, the magnitude of restoring moment in the dynamic condition is smaller than the hydrostatic condition, and it is vice-versa towards the higher wave frequencies. It was observed that the wave exciting moment induced on the model in one-half cycle has positive values and turns into negative values in the following half cycle; and the maximum value is achieved when the model is at a surface elevation of zero (heave motion is zero), which is due to a maximum slope of the free surface.

The magnitude of roll added mass moment of inertia coefficient varies at different wave frequencies (Figure 7.6). At a low wave frequency, the coefficient has a negative value, which is interpreted as resisting the roll motion because the flow acceleration around the model is dominant and is in the opposite direction of the rolling motion. While, at higher wave frequencies, the coefficients are positive and contribute to the roll motion development. Although, the magnitude of roll added mass moment of inertia coefficients at different wave heights are the same for some frequencies, the magnitude of their moments around the resonance frequency and for the larger wave height is greater.

It was observed that there is a nonlinear relationship between the magnitude of roll damping, and wave height and frequency. The roll damping coefficient around the resonance frequency is larger than other frequencies, and the magnitude of roll damping increases at the larger wave heights investigated (Figure 7.8).

The findings demonstrate the importance of calculating roll hydrodynamic coefficients using a dynamic approach. This study introduced new approaches for accurate calculation of roll added mass moment of inertia, roll damping and roll restoring moments both in calm water and wave conditions considering the impacts of effective parameters. These approaches can be used to compute the roll hydrodynamic coefficients of other ship types and they are useful for ships' designers and operators to develop an accurate equation-based method to predict a ship behaviour in real sea condition and to investigate dynamic stability of the ship.

8.4 Suggestions for future works

This study contributes in several ways to the understanding of ship stability and provides a basis for considering dynamic behaviour in operational conditions. This work can be extended by:

- Further research can use the suggested methodology in this thesis to explore the sensitivity of different hull forms to variation of the roll resorting and exciting moments as well as the roll added mass moment of inertia and roll damping moment.
- Calculation of the roll hydrodynamic coefficients in irregular waves through experimental and numerical simulations can be investigated.
- Numerical investigation of scale effects on the magnitude of roll hydrodynamic coefficients in regular and irregular waves can be investigated.
- Developing mathematical models to predict the roll motion in regular and irregular waves considering roll hydrodynamic coefficients calculated from the proposed methods in this study.

References

AHMED, T., HUDSON, D. & TEMAREL, P. 2010. An investigation into parametric roll resonance in regular waves using a partly non-linear numerical model. *Ocean Engineering,* 37**,** 1307-1320.

AVALOS, G. O., WANDERLEY, J. B., FERNANDES, A. C. & OLIVEIRA, A. C. 2014. Roll damping decay of a FPSO with bilge keel. *Ocean Engineering,* 87**,** 111-120.

BAČKALOV, I., BULIAN, G., CICHOWICZ, J., ELIOPOULOU, E., KONOVESSIS, D., LEGUEN, J.-F., ROSÉN, A. & THEMELIS, N. 2016. Ship stability, dynamics and safety: Status and perspectives from a review of recent STAB conferences and ISSW events. *Ocean Engineering,* 116**,** 312-349.

BANGUN, E., WANG, C. & UTSUNOMIYA, T. 2010. Hydrodynamic forces on a rolling barge with bilge keels. *Applied Ocean Research,* 32**,** 219-232.

BASS, D. & HADDARA, M. 1988. Nonlinear models of ship roll damping. *International Shipbuilding Progress,* 35**,** 5-24.

BASSLER, C. C. 2013. *Analysis and modeling of hydrodynamic components for ship roll motion in heavy weather.* Virginia Tech.

BASSLER, C. C., BELENKY, V., BULIAN, G., FRANCESCUTTO, A., SPYROU, K. & UMEDA, N. 2011. Review of available methods for application to second level vulnerability criteria. *Contemporary ideas on ship stability and capsizing in waves.* Springer.

BEGOVIC, E., DAY, A. H., INCECIK, A., MANCINI, S. & PIZZIRUSSO, D. Roll damping assessment of intact and damaged ship by CFD and EFD methods. Proceedings of the 12th international conference on the stability of ships and ocean vehicles, 2015. 14-19.

BELENKY, V., BASSLER, C. & SPYROU, K. Dynamic stability assessment in early-stage ship design. Proceedings of the 10th International Conference on Stability of Ships and Ocean Vehicles, St. Petersburg, Russia, 2009.

BELENKY, V., BASSLER, C. G. & SPYROU, K. J. 2011. Development of second generation intact stability criteria. Naval surface warfare center carderock div bethesda md hydromechanics dept

BHATTACHARYYA, R. 1978. *Dynamics of marine vehicles*, John Wiley & Sons Inc.

BIKDASH, M., BALACHANDRAN, B. & NAVFEH, A. 1994. Melnikov analysis for a ship with a general roll-damping model. *Nonlinear Dynamics,* 6**,** 101-124.

BLUME, P. 1979. Experimentelle Bestimmung von Koeffizienten der wirksamen Rolldämpfung und ihre Anwendung zur Abschätzung extremer Rollwinkel. *Schiffstechnik,* 26**,** 3-23.

BU, S. X., GU, M. & ABDEL-MAKSOUD, M. 2019. Study on Roll Restoring Arm Variation Using a Three-Dimensional Hybrid Panel Method. *Journal of Ship Research*.

BULIAN, G. 2008. On an improved Grim effective wave. *Ocean Engineering,* 35**,** 1811-1825.

BULIAN, G. & FRANCESCUTTO, A. 2006. Safety and operability of fishing vessels in beam and longitudinal waves. *International Journal of Small Craft Technology,* 148**,** 1-16.

BULIAN, G. & FRANCESCUTTO, A. 2007. On the effect of stochastic variations of restoring moment in long-crested irregular longitudinal sea. *International Shipbuilding Progress,* 54**,** 227-248.

BULIAN, G., FRANCESCUTTO, A., BULIAN, G. & FRANCESCUTTO, A. Considerations on parametric roll and dead ship conditions for the development of second generation intact stability criteria. Proc. 12th International Ship Stability Workshop, Washington, USA, 2011.

BULIAN, G., FRANCESCUTTO, A. & LUGNI, C. 2006. Theoretical, numerical and experimental study on the problem of ergodicity and 'practical ergodicity'with an application to parametric roll in longitudinal long crested irregular sea. *Ocean engineering,* 33**,** 1007-1043.

BULIAN, G., FRANCESCUTTO, A., UMEDA, N. & HASHIMOTO, H. 2008. Qualitative and quantitative characteristics of parametric ship rolling in random waves in the light of physical model experiments. *Ocean Engineering,* 35**,** 1661-1675.

CD-ADAPCO, S. 2015. STAR CCM+ user guide version 10.04. CD-adapco New York.

DAS, S., SAHOO, P. & DAS, S. 2006. Determination of roll motion for a floating body in regular waves. *Proceedings of the Institution of Mechanical Engineers, Part M: Journal of Engineering for the Maritime Environment,* 220**,** 41-48.

DISCUSSER, O., MUMM, H., DISCUSSERS, F., MOROOKA, C., PESCE, C. P., IVALDI, A., CHIRICA, I., RIZZUTO, E., BAARHOLM, G. S. & CHO, D. S. DYNAMIC RESPONSE. 18TH INTERNATIONAL SHIP AND OFFSHORE STRUCTURES CONGRESS, 2014.

DUNWOODY, A. B. 1989. ROLL OF A SHIP IN ASTERN SEAS--METACENTRIC HEIGHT SPECTRA. *Journal of ship research,* 33.

E SILVA, S. R. & SOARES, C. G. 2013. Prediction of parametric rolling in waves with a time domain non-linear strip theory model. *Ocean Engineering,* 72**,** 453-469.

FERZIGER, J. H., PERIC, M. & LEONARD, A. 1997. Computational methods for fluid dynamics. AIP.

FIELD, P. L. 2013. *Comparison of RANS and Potential Flow Force Computations for the ONR Tumblehome Hullfrom in Vertical Plane Radiation and Diffraction Problems.* Virginia Tech.

FRANCE, W. N., LEVADOU, M., TREAKLE, T. W., PAULLING, J. R., MICHEL, R. K. & MOORE, C. 2003. An investigation of head-sea parametric rolling and its influence on container lashing systems. *Marine Technology,* 40**,** 1-19.

FRANCESCUTTO, A. & UMEDA, N. Current status of new generation intact stability criteria development. Proceedings of the 11th International Ship Stability Workshop, Wageningen, The Netherlands, 2010. 21-23.

GAO, Q. & VASSALOS, D. Numerical study of the roll decay of intact and damaged ships. 12th International Ship Stability Workshop, 2011.

GRINNAERT, F., BILLARD, J.-Y. & LAURENS, J.-M. 2016. KGmax curves associated with second generation intact stability criteria for different types of ships. *Journal of Marine Science and Application,* 15**,** 223-235.

GU, M., LU, J. & WANG, T. Experimental and numerical study on stability under dead ship condition of a tumblehome hull. 13th International Ship Stability Workshop, Brest, 2013.

H. ENSHAEI, S. S. K. 2018. Quantifying Ship's Dynamic Stability through Numerical Investigation of Weight Distribution. *Proceedings of the 13th Int. Conference on the Stability of Ships and Ocean Vehicles (STAB), Kobe, Japan*.

HANDSCHEL, S. & ABDEL-MAKSOUD, M. 2014. Improvement of the Harmonic Excited Roll Motion Technique for Estimating Roll Damping. *Ship Technology Research,* 61**,** 116-130.

HASHIMOTO, H. Experimental and numerical studies of parametric roll of a post-Panamax container ship in irregular waves. Proceedings of the 9th international conference on stability of ships and ocean vehicles, 2006, 2006. COPPE, 181-190.

HASHIMOTO, H. & UMEDA, N. 2004. Nonlinear analysis of parametric rolling in longitudinal and quartering seas with realistic modeling of roll-restoring moment. *Journal of Marine Science and Technology,* 9**,** 117-126.

HOLDEN, C., GALEAZZI, R., RODRÍGUEZ, C., PEREZ, T., FOSSEN, T. I., BLANKE, M. & DE ALMEIDA SANTOS NEVES, M. 2007. Nonlinear container ship model for the study of parametric roll resonance. *Modeling, identification and control,* 28**,** 87-103.

HUA, J., WANG, W.-H. & CHANG, J.-R. 1999. A representation of GM-variation in waves by the Volterra system. *Journal of marine science and technology,* 7**,** 94-100.

IKEDA, Y., HIMENO, Y. & TANAKA, N. 1978. A prediction method for ship roll damping. *Report of the Department of Naval Architecture, University of Osaka Prefecture*.

IRKAL, M. A., NALLAYARASU, S. & BHATTACHARYYA, S. 2016. CFD approach to roll damping of ship with bilge keel with experimental validation. *Applied Ocean Research,* 55**,** 1-17.

IRKAL, M. A., NALLAYARASU, S. & BHATTACHARYYA, S. 2019. Numerical prediction of roll damping of ships with and without bilge keel. *Ocean Engineering,* 179**,** 226-245.

ITTC 2011. Guidelines: Practical Guidelines for Ship CFD Applications. *ITTC Report***,** 7.5-03.

JAOUEN, F., KOOP, A. & VAZ, G. Predicting roll added mass and damping of a ship hull section using CFD. OMAE, 2011. 2011.

JIN, Y., CHAI, S., DUFFY, J., CHIN, C., BOSE, N. & TEMPLETON, C. 2016. RANS prediction of FLNG-LNG hydrodynamic interactions in steady current. *Applied Ocean Research,* 60**,** 141-154.

JUDGE, C. Frequency dependence of hydrodynamic coefficients in roll. Proceedings of the 29th American Towing Tank Conference, Annapolis, MD, 2010. 285-290.

JUDGE, C. Q. & JUDGE, J. A. 2013. Measurement of hydrodynamic coefficients on a planing hull using forced roll oscillations. *Journal of Ship Research,* 57**,** 112-124.

JUNG, K. H., CHANG, K.-A. & HUANG, E. T. 2005. Two-dimensional flow characteristics of wave interactions with a free-rolling rectangular structure. *Ocean Engineering,* 32**,** 1-20.

KAWAHARA, Y., MAEKAWA, K. & IKEDA, Y. 2012. A simple prediction formula of roll damping of conventional cargo ships on the basis of Ikeda's method and its limitation. *Journal of Shipping and Ocean Engineering,* 2**,** 201.

KAYDıHAN, L., UĞURLU, B. & ERGIN, A. 2011. A hydroelastic investigation into the dynamic response characteristics of bulk carriers. *Advances in Marine Structures***,** 33.

KERWIN, J. 1955. Note on rolling in longitudinal waves. *Int Shipbuild Prog,* 2**,** 597-614.

KIANEJAD, S., ENSHAEI, H., DUFFY, J. & ANSARIFARD, N. 2019a. Investigation of a ship resonance through numerical simulation. *Journal of Hydrodynamics***,** 1-15.

KIANEJAD, S., ENSHAEI, H., DUFFY, J. & ANSARIFARD, N. 2019b. Prediction of a ship roll added mass moment of inertia using numerical simulation. *Ocean Engineering,* 173**,** 77-89.

KIANEJAD, S., ENSHAEI, H. & RANMUTHUGALA, D. Estimation of added mass moment of inertia in roll motion through numerical simulation. PACIFIC 2017 International Maritime Conference, 2017. 1-15.

KIANEJAD, S., LEE, J., LIU, Y. & ENSHAEI, H. 2018. Numerical Assessment of Roll Motion Characteristics and Damping Coefficient of a Ship. *Journal of Marine Science and Engineering,* 6**,** 101.

KIANEJAD, S. S., ENSHAEI, H., DUFFY, J., ANSARIFARD, N. & RANMUTHUGALA, D. 2019c. Ship Roll Damping Coefficient Prediction Using CFD. *Journal of Ship Research*.

KIM, Y. & HERMANSKY, G. 2014. Uncertainties in seakeeping analysis and related loads and response procedures. *Ocean Engineering,* 86**,** 68-81.

KINNAS, S. A., YI-HSIANG, Y. & VINAYAN, V. Prediction of flows around FPSO hull sections in roll using an unsteady Navier-Stokes solver. The Sixteenth International Offshore and Polar Engineering Conference, 2006. International Society of Offshore and Polar Engineers.

KUBO, T., UMEDA, N., IZAWA, S. & MATSUDA, A. Total stability failure probability of a ship in irregular beam wind and waves: model experiment and numerical simulation. Proceedings of 11th International Conference on the Stability of Ships and Ocean Vehicles. Athens, Greece, 2012. 39-46.

MANCINI, S., BEGOVIC, E., DAY, A. H. & INCECIK, A. 2018. Verification and validation of numerical modelling of DTMB 5415 roll decay. *Ocean Engineering,* 162**,** 209-223.

MATUSIAK, J. On the effects of wave amplitude, damping and initial conditions on the parametric roll resonance. Proceedings of the 8th International Conference on Stability of Ships and Ocean Vehicles, Madrid, Spain, 2003. 341-348.

MCGOLDRICK, R. T. 1960. Ship vibration. DTIC Document.

MCTAGGART, K., DE KAT, J. O., HOGBEN, N., ROWE, S. J., KUO, C., KENDRICK, A., DINOVITZER, A., BUCKLEY, W. H., SAMES, P. C. & SCHELLIN, T. E. 2000. Capsize risk of intact frigates in irregular seas. Discussion. Authors' closure. *Transactions-Society of Naval Architects and Marine Engineers,* 108**,** 147-177.

MIN, G., JIANG, L. & WANG, T.-H. 2015. Stability of a tumblehome hull under the dead ship condition. *Journal of Hydrodynamics, Ser. B,* 27**,** 452-457.

MOCTAR, O. E., SHIGUNOV, V. & ZORN, T. 2012. Duisburg Test Case: Post-panamax container ship for benchmarking. *Ship Technology Research,* 59**,** 50-64.

MUNIF, A. & UMEDA, N. 2000. Modeling extreme roll motions and capsizing of a moderate-speed ship in astern waves. *Journal of the Society of Naval Architects of Japan,* 2000**,** 51-58.

NA, J. H., LEE, W. C., SHIN, H. S. & PARK, I. K. A design of bilge keels for harsh environment FPSOs. The Twelfth International Offshore and Polar Engineering Conference, 2002. International Society of Offshore and Polar Engineers.

NEVES, M., PÉREZ, N. & VALERIO, L. 1999. Stability of small fishing vessels in longitudinal waves. *Ocean Engineering,* 26**,** 1389-1419.

NEVES, M. A. On the excitation of combination modes associated with parametric resonance in waves. Proceedings of the 6th International Ship Stability Workshop, 2002.

NEVES, M. A., PÉREZ, N. & LORCA, O. Experimental analysis on parametric resonance for two fishing vessels in head seas. Proceedings of the 6th International Ship Stability Workshop, 2002.

NEVES, M. A. & RODRÍGUEZ, C. 2005. A non-linear mathematical model of higher order for strong parametric resonance of the roll motion of ships in waves. *Marine Systems & Ocean Technology,* 1**,** 69-81.

OH, I., NAYFEH, A. & MOOK, D. 2000. A theoretical and experimental investigation of indirectly excited roll motion in ships. *Philosophical Transactions of the Royal Society of London A: Mathematical, Physical and Engineering Sciences,* 358**,** 1853-1881.

OLIVA-REMOLA, A., BULIAN, G. & PÉREZ-ROJAS, L. 2018. Estimation of damping through internally excited roll tests. *Ocean Engineering,* 160**,** 490-506.

PALMQUIST, M. 1994. On the statistical properties of the metacentric height of ships in following seas.

PATERSON, E. G., WILSON, R. V. & STERN, F. 2003. General-purpose parallel unsteady RANS ship hydrodynamics code: CFDShip-Iowa. DTIC Document.

PAULLING, J. 1961. The tranverse Stability of a Ship in a Longitudinal Seaway. *Journal of Ship Research, SNAME,* 4**,** 37-49.

PAULLING, J. & ROSENBERG, R. 1959. On unstable ship motions resulting from nonlinear coupling. *Journal of Ship Research,* 3**,** 36-46.

PETERS, W. S., BELENKY, V. & BASSLER, C. On Vulnerability Criteria for Righting Lever Variations in Waves. Proc. 11th Int'l Ship Stability Workshop, 2010. 7-16.

PROCEDURES, I.-R. Guidelines. 2011. *Practical Guidelines for Ship CFD Applications***,** 1-18.

REED, A. M. 26th ITTC parametric roll benchmark study. 12th International Ship Stability Workshop, 2011.

RIBEIRO E SILVA, S. & GUEDES SOARES, C. Time domain simulation of parametrically excited roll in head seas. Proceedings of the 7th International Conference of Ships and Ocean Vehicles (STAB'2000), Launceston, Tasmania, Australia, 2000. 652-664.

RIBEIRO E SILVA, S. & GUEDES SOARES, C. Parametric Rolling of a Container Vessel in Longitudinal Waves. Proc. 10th Int'l Conf. Stability of Ships & Ocean Vehicles, 2009.

RODDIER, D., LIAO, S.-W. & YEUNG, R. 2000. Wave-induced motion of floating cylinders fitted with bilge keels. *International Journal of Offshore and Polar Engineering,* 10.

RUSCHE, H. 2003. *Computational fluid dynamics of dispersed two-phase flows at high phase fractions.* Imperial College London (University of London).

S. S. KIANEJAD, H. E., J. DUFFY,N. ANSARIFARD 2018a. Calculation of Restoring Moment in Ship roll motion through Numerical Simulation. *Proceedings of the 13th Int. Conference on the Stability of Ships and Ocean Vehicles (STAB), Kobe, Japan*.

S. S. KIANEJAD, H. E., J. DUFFY,N. ANSARIFARD, D. RANMUTHUGALA 2018b. Investigation of scale effects on roll damping through numerical simulations. *Proceedings of the 32nd Symposium on Naval Hydrodynamics, Hamburge, Germany*.

SALVESEN, N., TUCK, E. & FALTINSEN, O. 1970. Ship motions and sea loads. *Trans. SNAME,* 78**,** 250-287.

SCHUMACHER, A., E SILVA, S. R. & SOARES, C. G. 2016. Experimental and numerical study of a containership under parametric rolling conditions in waves. *Ocean Engineering,* 124**,** 385-403.

SHIGUNOV, V., RATHJE, H., EL MOCTAR, O., ALTMAYER, B. & LLOYD, G. On the Consideration of Lateral Accelerations in Ship Design Rules. Proc. 12th International Ship Stability Workshop, Washington, USA, 2011.

SHIN, Y., BELENKY, V., PAULLING, J., WEEMS, K., LIN, W., MCTAGGART, K., SPYROU, K. J., TREAKLE, T. W., LEVADOU, M. & HUTCHISON, B. L. 2004. Criteria for parametric roll of large containerships in longitudinal seas. Discussion. *Transactions-Society of Naval Architects and Marine Engineers,* 112**,** 14-47.

SILVA, S., SANTOS, T. & SOARES, C. G. 2005. Parametrically excited roll in regular and irregular head seas. *International Shipbuilding Progress,* 52**,** 29-56.

SIMONSEN, C. D., OTZEN, J. F., JONCQUEZ, S. & STERN, F. 2013. EFD and CFD for KCS heaving and pitching in regular head waves. *Journal of Marine Science and Technology,* 18**,** 435-459.

SOLIMAN, M. S. & THOMPSON, J. Indeterminate sub-critical bifurcations in parametric resonance. Proceedings of the Royal Society of London A: Mathematical, Physical and Engineering Sciences, 1992. The Royal Society, 511-518.

SOMAYAJULA, A. & FALZARANO, J. 2017a. Application of advanced system identification technique to extract roll damping from model tests in order to accurately predict roll motions. *Applied Ocean Research,* 67**,** 125-135.

SOMAYAJULA, A. & FALZARANO, J. 2018. Volterra approach–a new method to accurately calculate the non-linear and time-varying roll restoring arm of ships in irregular longitudinal seas. *Ships and Offshore Structures,* 13**,** 423-431.

SOMAYAJULA, A., GUHA, A., FALZARANO, J., CHUN, H.-H. & JUNG, K. H. 2014. Added resistance and parametric roll prediction as a design criteria for energy efficient ships. *Ocean Systems Engineering,* 4**,** 117-136.

SOMAYAJULA, A. S. & FALZARANO, J. 2017b. A comparative assessment of simplified models for simulating parametric roll. *Journal of Offshore Mechanics and Arctic Engineering,* 139**,** 021103.

SOMAYAJULA, A. S. & FALZARANO, J. M. Validation of volterra series approach for modelling parametric rolling of ships. ASME 2015 34th International Conference on Ocean, Offshore and Arctic Engineering, 2015. American Society of Mechanical Engineers, V011T12A043-V011T12A043.

SONG, K.-H., KIM, Y. & PARK, D.-M. 2013. Quantitative and qualitative analyses of parametric roll for ship design and operational guidance. *Proceedings of the Institution of Mechanical Engineers, Part M: Journal of Engineering for the Maritime Environment,* 227**,** 177-189.

SPYROU, K., TIGKAS, I., SCANFERLA, G., PALLIKAROPOULOS, N. & THEMELIS, N. 2008. Prediction potential of the parametric rolling behaviour of a post-panamax containership. *Ocean Engineering,* 35**,** 1235-1244.

STERN, F., WILSON, R. & SHAO, J. 2006. Quantitative V&V of CFD simulations and certification of CFD codes. *International journal for numerical methods in fluids,* 50**,** 1335-1355.

STERN, F., WILSON, R. V., COLEMAN, H. W. & PATERSON, E. G. 2001. Comprehensive approach to verification and validation of CFD simulations-Part 1: methodology and procedures. *Transactions-American Society of Mechanical Engineers Journal of Fluids Engineering,* 123**,** 793-802.

SUBRAMANIAN, R. 2012. *A time domain strip theory approach to predict maneuvering in a seaway.* University of Michigan.

TAYLAN, M. 2003. Static and dynamic aspects of a capsize phenomenon. *Ocean engineering,* 30**,** 331-350.

TEZDOGAN, T., DEMIREL, Y. K., KELLETT, P., KHORASANCHI, M., INCECIK, A. & TURAN, O. 2015. Full-scale unsteady RANS CFD simulations of ship behaviour and performance in head seas due to slow steaming. *Ocean Engineering,* 97**,** 186-206.

THEIN, Z. 2012. *Practical Source Code for Ship Motions Time Domain Numerical Analysis and Its Mobile Device Application.* Chalmers university of technology.

THEMELIS, N., SPYROU, K. J., AYYUB, B. M., FRANCESCUTTO, A., BULIAN, G., MYRHAUG, D., AALL DAHLE, E., UMEDA, N. & BELENKY, V. 2007. Probabilistic assessment of ship stability. Discussion. *Transactions-Society of Naval Architects and Marine Engineers,* 115**,** 181-206.

THIAGARAJAN, K. P. & BRADDOCK, E. C. 2010. Influence of bilge keel width on the roll damping of FPSO. *Journal of Offshore Mechanics and Arctic Engineering,* 132**,** 011303.

TONG, Z., ZHANG, Y., ZHANG, Z. & HUA, H. 2007. Dynamic behavior and sound transmission analysis of a fluid–structure coupled system using the direct-BEM/FEM. *Journal of Sound and Vibration,* 299**,** 645-655.

UMEDA, N. Current status of second generation intact stability criteria development and some recent efforts. Proceedings of the 13th International Ship Stability Workshop, Brest, 2013. 23-26.

UMEDA, N., HASHIMOTO, H., VASSALOS, D., URANO, S. & OKOU, K. 2004. Nonlinear dynamics on parametric roll resonance with realistic numerical modelling. *International shipbuilding progress,* 51**,** 205-220.

UMEDA, N., IZAWA, S., SANO, H., KUBO, H., YAMANE, K. & MATSUDA, A. Validation attempts on draft new generation intact stability criteria. Proc. 12th International Ship Stability Workshop, Washington, USA, 2011.

UMEDA, N., KAWAIDA, D., ITO, Y., TSUTSUMI, Y., MATSUDA, A. & TERADA, D. Remarks on Experimental Validation Procedures for Numerical Intact Stability Assessment with Latest Examples. International Ship Stability Workshop, 2014. 77-84.

UMEDA, N., SAKAI, M., FUJITA, N., MORIMOTO, A., TERADA, D. & MATSUDA, A. 2016. Numerical prediction of parametric roll in oblique waves. *Ocean Engineering,* 120**,** 212-219.

VERNON, T. A., BARA, B. & HALLY, D. 1988. A surface panel method for the calculation of added mass matrices for finite element models. DTIC Document.

VIDIC-PERUNOVIC, J. 2011. Influence of the GZ calculation method on parametric roll prediction. *Ocean Engineering,* 38**,** 295-303.

WASSERMANN, S., FEDER, D.-F. & ABDEL-MAKSOUD, M. 2016. Estimation of ship roll damping—A comparison of the decay and the harmonic excited roll motion technique for a post panamax container ship. *Ocean Engineering,* 120**,** 371-382.

WAWRZYŃSKI, W. & KRATA, P. 2016. On ship roll resonance frequency. *Ocean Engineering,* 126**,** 92-114.

WILKEN, M., MENK, A., VOSS, H. & CABOS, C. 2011. Efficient calculation of fluid structure interaction in ship vibration. *Advances in Marine Structures, London***,** 75-85.

WILKEN, M., OF, G., CABOS, C. & STEINBACH, O. 2009. Efficient calculation of the effect of water on ship vibration. *Analysis and Design of Marine Structures. Proceedings of MARSTRUCT***,** 93-101.

WILSON, R. V., CARRICA, P. M. & STERN, F. 2006. Unsteady RANS method for ship motions with application to roll for a surface combatant. *Computers & fluids,* 35**,** 501-524.

WRIGHT, J. & MARSHFIELD, W. 1979. Ship roll response and capsize behaviour in beam seas.

YANG, C.-L., ZHU, R.-C., MIAO, G.-P. & JU, F. 2013. Numerical simulation of rolling for 3-D ship with forward speed and nonlinear damping analysis. *Journal of Hydrodynamics, Ser. B,* 25**,** 148-155.

YI-HSIANG, Y., KINNAS, S. A., VINAYAN, V. & KACHAM, B. K. Modeling of flow around FPSO hull sections subject to roll motions: Effect of the separated flow around bilge keels. The Fifteenth International Offshore and Polar Engineering Conference, 2005. International Society of Offshore and Polar Engineers.

YU, Y.-H. & KINNAS, S. A. 2009. Roll response of various hull sectional shapes using a Navier-Stokes solver. *International Journal of Offshore and Polar Engineering,* 19.

ZHOU, Y.-H., NING, M., XUN, S. & ZHANG, C. 2015. Direct calculation method of roll damping based on three-dimensional CFD approach. *Journal of Hydrodynamics, Ser. B,* 27**,** 176-186.

Appendix